November 22, 1967

To the Graduate Council:

I am submitting herewith a thesis written by Donald Edward Chriss entitled "An Experimental Study of the Turbulent Mixing of Subsonic Axisymmetric Gas Streams." I recommend that it be accepted for nine quarter hours of credit in partial fulfillment of the requirements for the degree of Master of Science, with a major in Mechanical Engineering.

Major Professor

We have read this thesis and recommend its acceptance:

Accepted for the Council:

Vice President for
Graduate Studies for Research

AN EXPERIMENTAL STUDY OF THE TURBULENT MIXING OF SUBSONIC AXISYMMETRIC GAS STREAMS

A Thesis

Presented to

the Graduate Council of

The University of Tennessee

In Partial Fulfillment

of the Requirements for the Degree

Master of Science

---

by

Donald Edward Chriss

December 1967

ACKNOWLEDGEMENT

The work described herein was performed under the provisions of United States Air Force Contract No. AF 40(600)-1200 with ARO, Inc., the operating contractor of the Arnold Engineering Development Center for the Air Force Systems Command. The writer is grateful to his employer for providing the resources necessary for this work and hopes that the results will be of value in the field of fluid mechanics research and development.

The writer expresses his appreciation to his associates, Messrs. C. E. Peters, R. P. Rhodes, Jr., and R. C. Bauer, for their assistance and comments which added materially to the quality of the work. Thanks are also extended to Miss S. Mercer for her conscientious efforts during the typing of the text. Miss A. Parker deserves a special acknowledgement for her extensive efforts with regard to the preparation of the entire manuscript. The writer is also grateful for the guidance received from Dr. S. C. Lee of The University of Missouri at Rolla, Rolla, Missouri (formerly of The University of Tennessee Space Institute, Tullahoma, Tennessee) and from Dr. J. M. Wu of The University of Tennessee Space Institute.

760898

TABLE OF CONTENTS

CHAPTER		PAGE
I.	INTRODUCTION	1
	General Discussion	1
	Objective and Justification	3
	Approach	6
II.	EXPERIMENTAL APPARATUS AND PROCEDURE	8
	Free Jet Mixing Test Cell	8
	Instrumentation	10
	Testing Procedure	13
	Data Reduction Procedure	15
III.	DISCUSSION OF RESULTS	17
	Flow Field Description	17
	Experimental Data	17
	Consistency Check	21
	Centerline Decay	25
	Profile Similarity	34
	Momentum and Energy Transport	43
	Composition and Energy Transport	47
	Static Pressure	49
IV.	CONCLUSIONS	52
V.	RECOMMENDATIONS AND PLANS FOR FURTHER STUDY	54
BIBLIOGRAPHY		56

CHAPTER PAGE

APPENDIXES. 58

APPENDIX A. 59

APPENDIX B. 65

LIST OF TABLES

TABLE		PAGE
I.	Test Conditions	19
II.	Nondimensionalizing Radii	39
III.	Measurement Accuracy.	60
IV.	Errors in Calculated Parameters	62
V.	Influence Coefficients for ψ_u	63

LIST OF FIGURES

FIGURE		PAGE
1.	Schematic Diagram of the Free Jet Mixing Test Cell.	9
2.	Dual Probe Arrangement.	11
3.	Probe Related Components.	12
4.	Free Jet Mixing Configuration	18
5.	Consistency Check for Series I Tests.	22
6.	Consistency Check for Series II Tests	23
7.	Centerline Composition Decay for the Hydrogen–Air Tests.	26
8.	Centerline Velocity Decay for the Hydrogen–Air Tests	27
9.	Centerline Velocity Decay for Constant Velocity Ratio Systems	28
10.	Centerline Composition Decay, Comparison with Zakkay's Result	30
11.	Potential Core Length versus Mass Flux Ratio. .	31
12.	Centerline Decay for Test II A.	32
13.	Centerline Decay for Test I B	33
14.	Radial Composition Profile.	35
15.	Radial Composition Profile, Comparison with Mathematical Functions.	36

FIGURE PAGE

16. Radial Velocity Profile 37

17. Radial Composition and Velocity Profiles for Tests I A and II A. 42

18. First Regime Radial Velocity Profile. 44

19. Velocity–Enthalpy Relationship for the Hydrogen–Air Tests. 45

20. Velocity–Enthalpy Relationship for the Air–Air Tests 46

21. Composition–Enthalpy Relationship for the Hydrogen–Air Tests. 48

22. Static Pressure Profiles for Test II B. 50

23. Static Pressure Profiles for Test II C. 51

NOMENCLATURE

b	Mixing zone width
C	Hydrogen mass fraction
C_p	Specific heat at constant pressure
D	Inner nozzle diameter
g	Dimensional constant
H	Enthalpy
H_h	Enthalpy of hydrogen
H_a	Enthalpy of air
M	Mach number
P	Pressure
Pr	Prandtl number
P_{TH}	Total pressure in the inner plenum chamber
R	Radius
R^*	Radius of control volume
R_{mc}	Radius at which $C = 0.5\ C_c$
R_{mu}	Radius at which $u = 0.5\ (u_c - u_o)$
$\bar{R}$	Universal gas constant
R_B	$\frac{R - R_{.9}}{R_{.1} - R_{.9}}$
R_i	Radius of the potential core
R_o	Radius of the inner nozzle
$R_{.9}$	Radius at which $u = 0.9\ (u_c - u_o)$

$R_{.1}$	Radius at which $u = 0.1\ (u_c - u_o)$
T	Temperature
T_{TH}	Total temperature in the inner plenum chamber
u	Velocity in the axial direction
v	Velocity in the radial direction
$\dot{W}$	Hydrogen mass flow rate from mass balance
$\dot{W}_j$	Hydrogen mass flow rate from metering orifice measurement
x	Axial distance
$\bar{x}$	x/x_o
x_o	Potential core length
x_{oc}	Potential core length from composition
x_{ou}	Potential core length from velocity
γ	Ratio of specific heats
ϵ	Eddy viscosity
λ	Mass flux ratio
ρ	Density
ϕ_H	$\frac{H - H_o}{H_j - H_o}$
ϕ_u	$\frac{u - u_o}{u_j - u_o}$
ψ_u	$\frac{u - u_o}{u_c - u_o}$
ω	Molecular weight

Subscripts

c	Centerline
j	Jet gas
o	Outer stream gas
s	Static
t	Total

CHAPTER I

INTRODUCTION

I. GENERAL DISCUSSION

The turbulent mixing between high-speed coaxial streams is of primary importance in many engineering devices, such as jet pumps, ejectors, and ramjet combustors. The flow in these devices must at best be analyzed by semi-empirical techniques because there is no fundamental and complete theory for turbulent flows. Numerous investigations of the turbulent mixing process have been conducted, but they have failed to produce a generalized theory. The main reason for the lack of success in solving this problem is that the turbulent mixing process is influenced by the local flow properties as well as the boundary conditions.

The case of a single jet mixing with a quiescent medium has been given considerable attention by a number of investigators. The results of these studies are well covered by Schlichting (1)[1] and Pai (2). One of the first investigations of the case of two moving streams

---

[1]Numbers in parentheses refer to similarly numbered references in the bibliography.

mixing together was conducted by Forstall and Shapiro (3). An inner stream composed of air with ten per cent by volume of helium as a tracer was mixed with an outer stream of air. The gas velocities were in the low subsonic range, and the temperatures were maintained nearly equal. The main conclusions were that [1] momentum diffuses less rapidly than mass, and [2] the normalized velocity and composition profiles exhibit shape similarity; that is, the nondimensional radial profiles are invariant with axial distance.

Alpinieri (4) obtained experimental data on the turbulent mixing between carbon dioxide and hydrogen central jets exhausting into a moving concentric stream of air. The flow velocities were in the low to high subsonic range, and the temperatures of the streams were approximately equal. Radial and axial distributions of composition and velocity were presented. Alpinieri concluded that no tendency toward segregation of the streams exists when either the velocities or the mass fluxes of the stream are equal. Conclusions contrary to this were suggested by turbulent eddy viscosity models proposed by other investigators such as Prandtl as presented by Schlichting (1) and Ferri (5). Also, Alpinieri verified Forstall and Shapiro's conclusion that mass diffuses more readily than momentum.

Zakkay and others (6) conducted an experimental investigation to determine the turbulent transport coefficients for hydrogen–, helium–, and argon–air mixing systems. Central jets of hydrogen, helium, and argon at subsonic velocities were injected into an outer stream of air maintained at a constant Mach number of 1.6. The ratio of the inner jet velocity to the outer stream velocity for the hydrogen–air mixing system was varied from 0.768 to 2.42. In addition to turbulent transport coefficients, centerline decay of velocity and composition was presented. Twelve major conclusions were drawn from this investigation by Zakkay. A few of these are discussed in Chapter III, in which results from Zakkay's investigation are compared with results obtained in the current investigation.

II. OBJECTIVE AND JUSTIFICATION

The objective of this experimental investigation was to document the turbulent mixing of subsonic axisymmetric hydrogen and air streams at velocity ratios which have not been previously reported. Special emphasis is placed on [1] determining the effect of velocity ratio and density gradients on the centerline decay of composition, velocity, and total enthalpy, and on the composition, velocity, and total enthalpy profile shapes, and [2] pre–

senting nondimensional composition, velocity, and total enthalpy relationships which are indicative of the turbulent Prandtl, Lewis, and Schmidt numbers.

Integral techniques for solving turbulent mixing problems (7, 8) assume that composition, velocity, and total enthalpy profiles exhibit shape similarity. Forstall and Shapiro (3) listed the following relationships as being representative of their velocity profile shapes:

Cosine curve

$$\frac{u - u_o}{u_c - u_o} = \frac{1}{2}\left(1 + \cos\frac{\pi R}{2 R_{mu}}\right),$$

Three-halves power curve

$$\frac{u - u_o}{u_c - u_o} = \left[1 - 0.293\,(R/R_{mu})^{3/2}\right]^2,$$

and

Error curve

$$\frac{u - u_o}{u_c - u_o} = \left[\frac{1}{2}\right](R/R_{mu})^2 .$$

If profile shape similarity is a valid assumption, a representative profile curve and the centerline and outer stream velocities are sufficient to determine the radial velocity distribution at any axial location.

In most proposed methods for solving turbulent mixing problems, the turbulent Prandtl and Lewis numbers are assumed to be unity to simplify the mathematical

procedure. If the Prandtl and Lewis numbers are unity, the Schmidt number must be unity by definition. For unity Prandtl and Lewis numbers, the laminar boundary layer equations for axisymmetric flow with the laminar transport properties replaced by the corresponding turbulent values may be written as follows:

Momentum equation,

$$\rho u \frac{\partial u}{\partial x} + \rho v \frac{\partial u}{\partial R} = \frac{1}{R} \frac{\partial}{\partial R} (\rho \epsilon R \frac{\partial u}{\partial R}) - \frac{\partial P}{\partial x} , \qquad [1]$$

Energy equation,

$$\rho u \frac{\partial H}{\partial x} + \rho v \frac{\partial H}{\partial R} = \frac{1}{R} \frac{\partial}{\partial R} (\rho \epsilon R \frac{\partial H}{\partial R}) , \qquad [2]$$

Conservation of elemental species,

$$\rho u \frac{\partial C}{\partial x} + \rho v \frac{\partial C}{\partial R} = \frac{1}{R} \frac{\partial}{\partial R} (\rho \epsilon R \frac{\partial C}{\partial R}) , \qquad [3]$$

and

Global continuity equation,

$$\frac{\partial (\rho u)}{\partial x} + \frac{1}{R} \frac{\partial (\rho v R)}{\partial R} = 0 . \qquad [4]$$

For the case of constant pressure mixing of an initially uniform infinite stream, the $\partial P/\partial x$ term in Equation [1] is zero, and Equations [1], [2], and [3] are identical in form. A linear relation may be obtained between the variables [u, H, and C] as follows:

$$\frac{u - u_o}{u_j - u_o} = \frac{H - H_o}{H_j - H_o} = \frac{C - C_o}{C_j - C_o} . \qquad [5]$$

The relationship between the terms of Equation [5] will be presented in this investigation as being indicative of the Prandtl and Lewis number variation.

III. APPROACH

In general, turbulent mixing is influenced by the following factors:

1. Velocity ratio between the streams,
2. Density gradients in the mixing region,
3. Axial and radial static pressure gradients, and
4. Initial boundary layer and free stream turbulence level.

The approach which has been taken in this investigation is to reduce the effect of initial boundary layer and static pressure gradients and to concentrate on the effects of velocity ratio and the density field. The initial boundary layer effect was reduced by designing the nozzles to minimize the boundary layer buildup at the entrance to the test section. This proved to be a lengthy experimental investigation in itself. The nozzles eventually selected for the mixing studies had essentially equal boundary layer thicknesses. The combined thickness of the inner and outer boundary layers at the nozzle exit plane was approximately seven per cent of the inner nozzle diameter. The static pressure variation was

minimized by exhausting to atmosphere as a free jet and maintaining the flows subsonic so that shock waves were not formed. However, the static pressure in the mixing region was measured, and the gradients in the near field region were larger than anticipated. The static pressure data are presented in Chapter III.

Hydrogen–air and air–air turbulent mixing systems were investigated. The hydrogen–air system was chosen to provide a system with very large density gradients. Also, the high speed of sound of hydrogen makes it possible to attain high velocity ratios while the Mach numbers remain subsonic. Furthermore, hydrogen–air mixtures are used in combustion processes, and the results should be useful when chemically reactive systems are investigated. The air–air system is studied because it provides a system with small density gradients to use for comparison with the high density gradient system.

The approach of this investigation required that a large amount of experimental data be obtained. These data were needed to develop semi–empirical techniques for solving turbulent mixing systems. The experimental measurements are time–mean average values because techniques for measuring the fluctuating quantities are not well developed especially in the high velocity region.

CHAPTER II

EXPERIMENTAL APPARATUS AND PROCEDURE

I. FREE JET MIXING TEST CELL

A schematic diagram of the free jet mixing test cell is shown in Figure 1. The inner nozzle is located inside the outer plenum. Air, which may be heated to 1500°R by an indirect fired heater, flows around the inner plenum and nozzle. The heated air from the outer plenum then passes through a 3.5 inch diameter subsonic nozzle to form an annulus around the subsonic flow from the inner nozzle. The inner nozzle diameter is 0.5 inch and the thickness of the trailing edge is 0.005 inch. The inner nozzle and outer nozzle configuration was designed to produce as small an initial boundary layer at the entrance to the test section as practical. The inner and outer nozzles were aligned to give flow with centerlines which are parallel within less than one-half degree. The alignment was checked by using total pressure measurements in the flow field. The test section is open to the atmosphere, but the gases from the nozzle are exhausted through a downstream scoop attached to the Rocket Test Facility exhaust system.

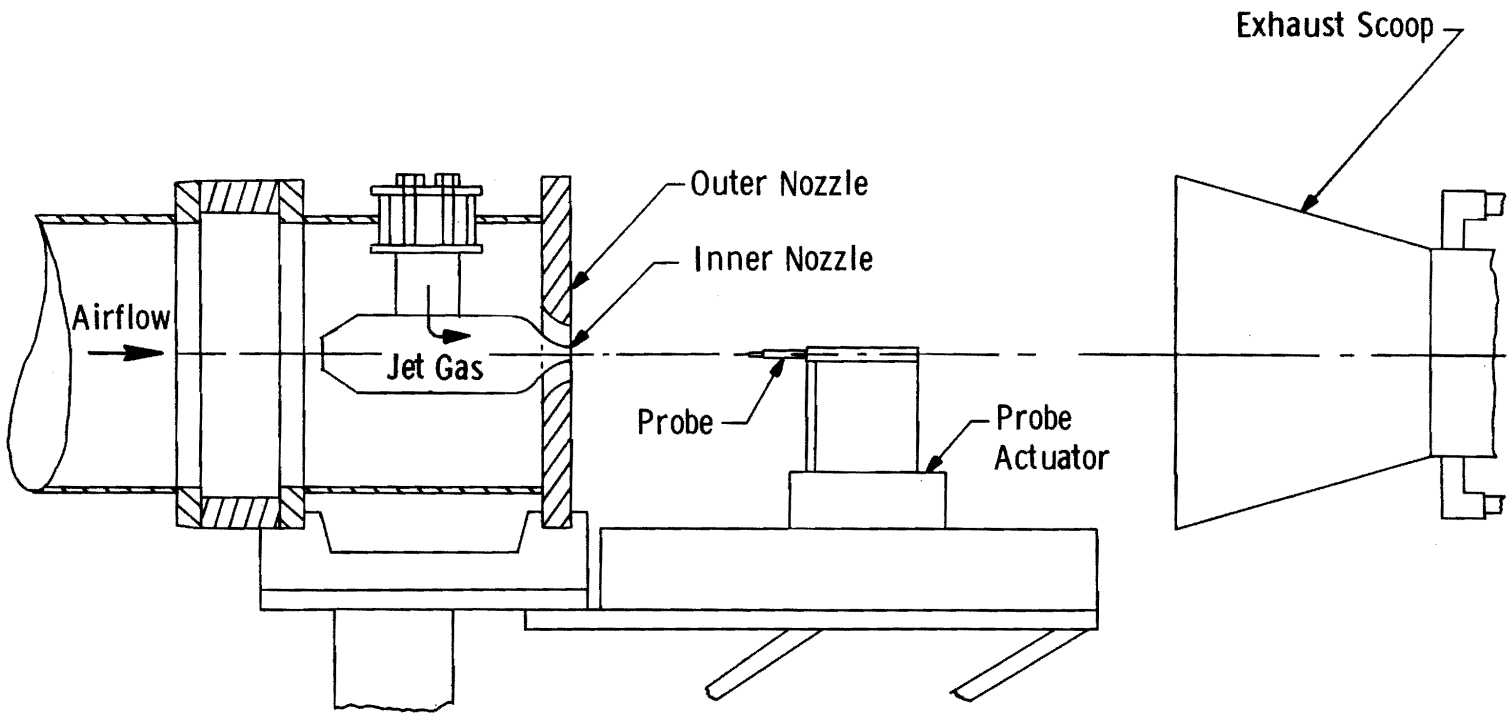

Figure 1. Schematic diagram of the free jet mixing test cell.

II. INSTRUMENTATION

A computer was used to record all of the data in millivolts on magnetic tape. The temperatures were measured on copper-constantan and iron-constantan thermocouples, and the pressures were measured on strain-gage-type transducers. The gas composition was measured by a fluid oscillator, which was developed by the Rocket Test Facility Research Branch. The operation of the fluid oscillator will be covered in an Arnold Engineering Development Center technical report to be published. The probe positions were measured on potentiometers, and the inner stream flow rate was measured by a calibrated choked orifice. Estimates of the accuracy of the measured parameters are presented in Appendix A.

A dual probe arrangement was used to measure the total pressure, total temperature, gas composition, and static pressure at various stations throughout the flow field. A photograph and a sketch of the dual probe arrangement are shown in Figure 2, and a schematic diagram of the probe related components is shown in Figure 3. The probe used to measure total pressure, total temperature, and gas composition is operated in two modes. Total temperature and gas composition are recorded on one mode when the probe is aspirated to a vacuum source, and

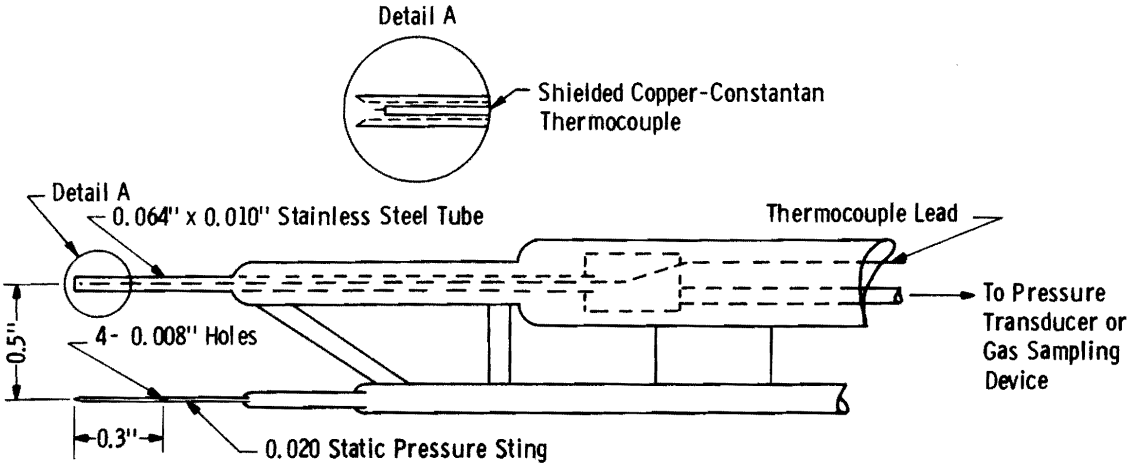

Figure 2. Dual probe arrangement.

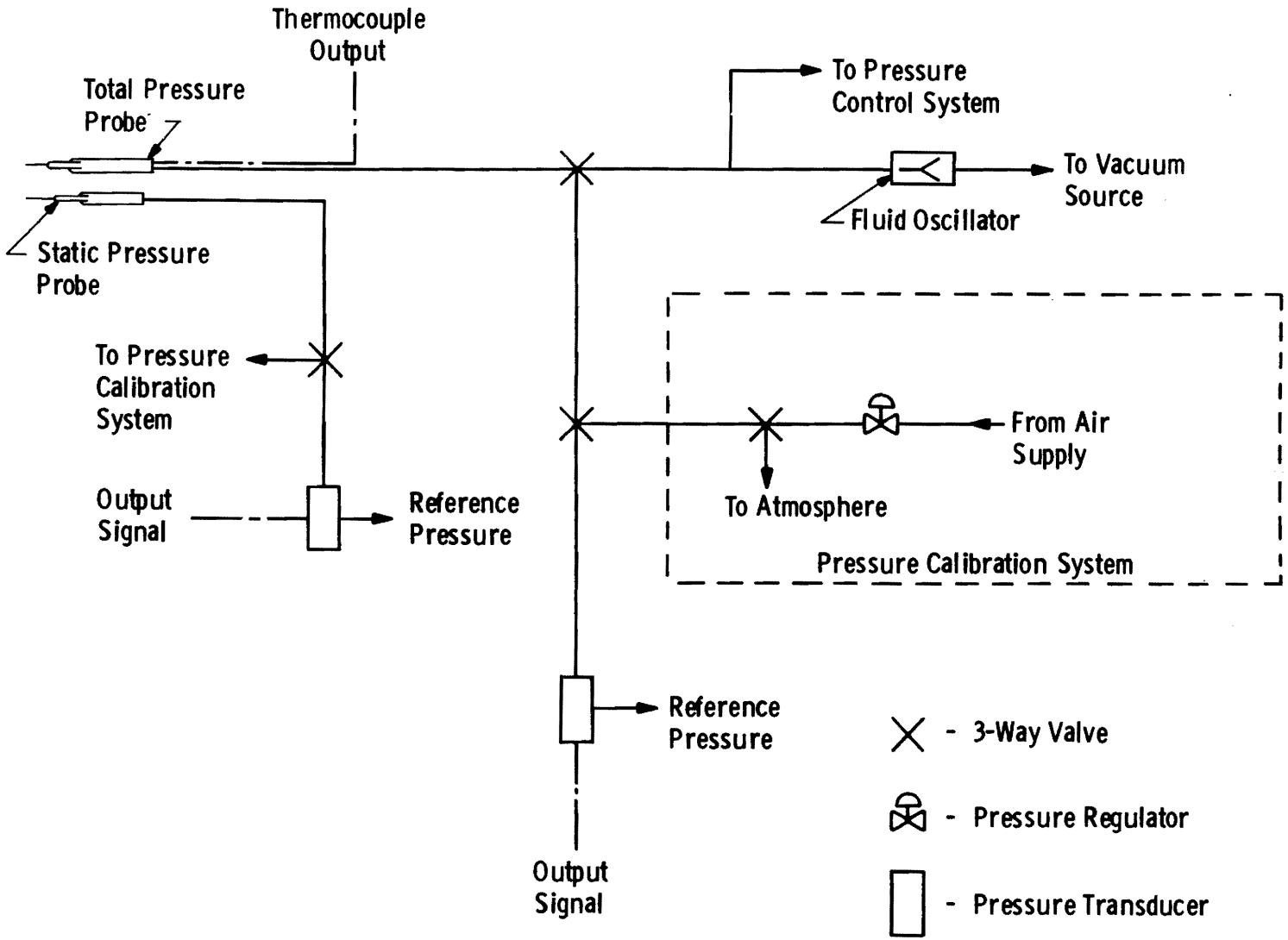

Figure 3. Probe related components.

total pressure is recorded on the other mode when there is no flow through the probe. Static pressure is recorded during both modes of operation. The static pressure measurements as recorded are displaced 0.5 inch to one side of the total pressure probe measurements. They are shifted in the data reduction program to align with the total pressure probe measurements.

The dual probe arrangement is actuated in the flow field by a three-position probe actuator. The probe location and the initial test conditions were monitored on a three-axis graphic recorder and strip-chart recorders.

III. TESTING PROCEDURE

In-place calibrations were made on all of the pressure transducers and potentiometers before each test. Temperature calibrations were provided by constant millivolt signal inputs to the temperature channels. Next, the test conditions were established by setting the total pressure in the inner and outer plenum chambers and the total temperature of the outer air stream. The conditions were allowed to stabilize, and then the probe was set on the vertical centerline of the flow field by the following procedure: The probe was located on the approximate horizontal centerline of the jet by using the peak of the horizontal total pressure profile. Then the probe was

moved to the decaying region of the jet and actuated vertically. The vertical centerline was taken to be the location of maximum pressure if the jet total pressure was greater than the outer stream total pressure or the minimum pressure if the jet total pressure was below the outer stream pressure.

The data were recorded by a data acquisition system which is operated in the following manner: The probe is traversed radially at a fixed axial location until the desired radial location is reached. A single switch starts a sequence which stops the probe and begins to record all of the data at a rate of 300 times per second. The probe is put into the total temperature and gas composition mode of operation then into the total pressure mode. The time in each mode of operation is indicated by a function signal switch recorded on magnetic tape. The magnetic tape drive is stopped automatically when all data at the radial location have been recorded. The probe drive is engaged automatically to traverse the probe to the next radial data point location selected by the test conductor. The total time required to obtain a data point in a radial survey is approximately five seconds. After data points have been recorded to give complete profiles at a given location, the radial traverse of the probe is

stopped, and the probe is moved to another axial location where the next radial profile is obtained.

IV. DATA REDUCTION PROCEDURE

The data are reduced in three steps with the aid of computers. First, the magnetic tape from the SEL 600 computer is processed through a data reduction program which uses the calibrations to convert the millivolt signals to engineering units of pressure, temperature, and probe position. The data are averaged over 0.167-second intervals to obtain the mean values. The data recorded during unstable conditions are eliminated. A printout and a tape are made of the remaining engineering units data.

Second, the engineering units tape is reduced by computer to give gas mixture properties. The properties obtained are composition, density, velocity, and total enthalpy at the initial stream conditions as well as at local points in the flow field. The methods of calculating the specific properties are given in Appendix B. These basic properties are recorded on the tape to be used as the inputs for the final reduction program. The method by which the data are further reduced may change as the knowledge of turbulent mixing increases. For this reason, the basic properties tape is stored so that other methods of data reduction may be applied to it.

Finally, the basic properties tape is reduced to provide profiles of nondimensionalized velocity, composition, and total enthalpy as well as relationships between these parameters which are representative of Prandtl and Lewis numbers. Also, a hydrogen mass balance is made at each axial station recorded by integrating the hydrogen mass flux [$\rho u C$] over the radial distance to a specified control volume.

CHAPTER III

DISCUSSION OF RESULTS

I. FLOW FIELD DESCRIPTION

The jet gas and the outer stream gas mix in the inner mixing zone as shown schematically in Figure 4. For all cases investigated, the jet gas used was either hydrogen or air at ambient temperature. Only regimes I and II are considered in this investigation. In regime III, the conditions in the outer stream are a function of the outer stream mixing with the quiescent air surrounding it. This provides a problem with more complex boundary conditions than the one under consideration. The potential core length varies with the test conditions. The core length is defined as the distance in which the centerline composition or velocity is the same as the inner nozzle exit conditions.

II. EXPERIMENTAL DATA

Experimental data were obtained for nine different test conditions. The velocities, total pressures, and total temperatures for these tests are tabulated in Table I. For the first five test conditions, Series I,

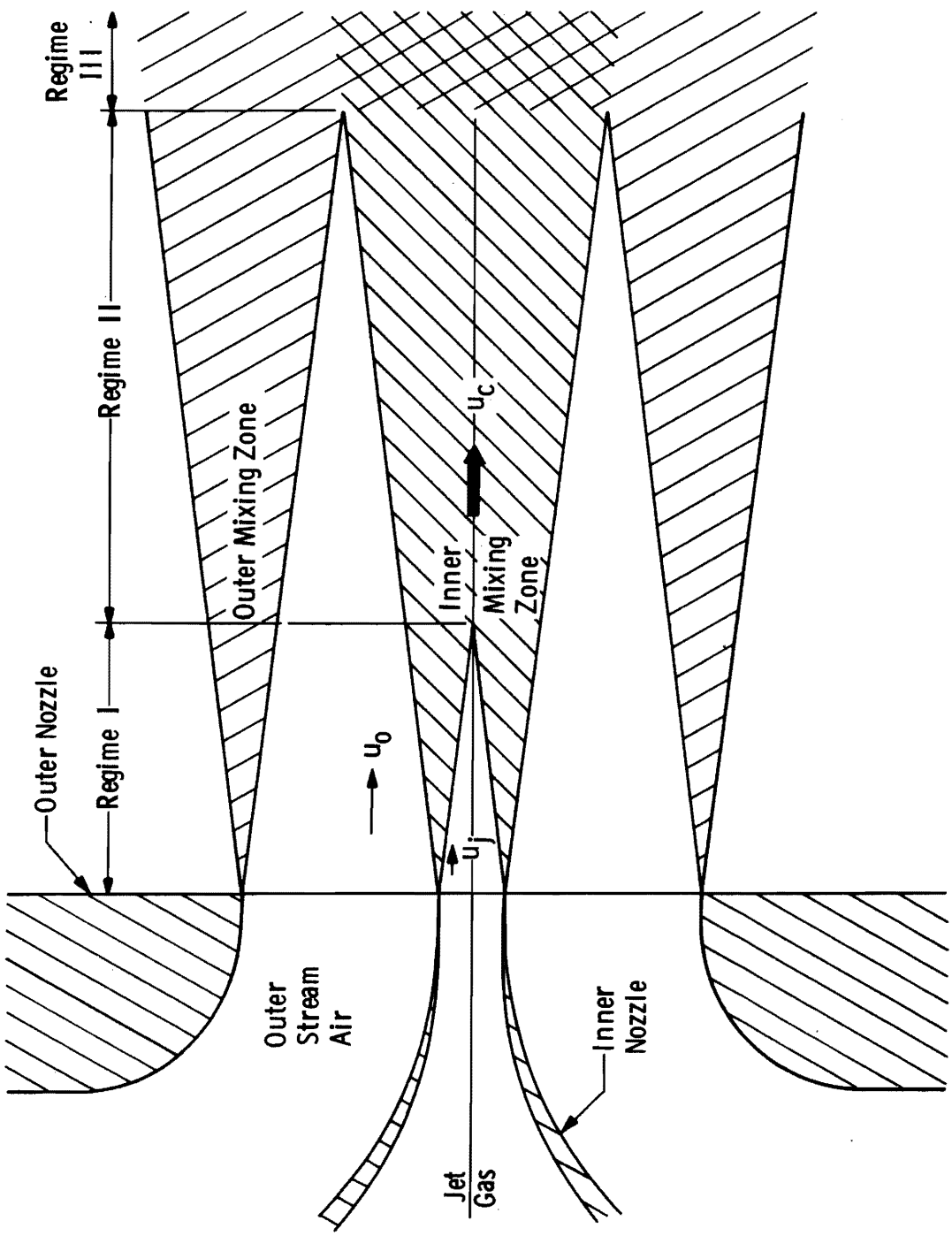

Figure 4. Free jet mixing configuration.

TABLE I

TEST CONDITIONS

Test No.	Jet Gas	Outer Stream Gas	u_j/u_o	u_j, ft/sec	P_{tj}, psfa	P_{to}, psfa	T_{tj}, °R	T_{to}, °R
I A	Hydrogen	Air	6.3	3300	3080	2325	550	650
I B	Hydrogen	Air	4.4	3200	3050	2610	550	650
I C	Hydrogen	Air	3.8	3050	2925	2760	550	650
I D	Hydrogen	Air	3.0	2400	2540	2765	550	650
I E	Hydrogen	Air	2.4	1900	2350	2760	550	650
II A	Hydrogen	Air	4.6	3100	2880	2325	550	1050
II B	Hydrogen	Air	3.2	2450	2530	2430	550	1050
II C	Hydrogen	Air	2.5	1950	2330	2435	550	1050
III	Air	Air	2.4	940	3395	2185	550	650

the total pressures of the two streams were set to give a range of velocity ratios from 2.4 to 6.3. In Series II, the next three test conditions, the main difference was that the outer stream temperature was raised from 650 to 1050°R. The total pressures were varied to give velocity ratios from 2.5 to 4.6. Series III, the last test condition, was an air-air mixing test at a velocity ratio of 2.4.

In the region very near the nozzle exit, the gradients of composition, total pressure, static pressure, and total temperature were very large. Insufficient data were obtained to define the profiles adequately because the increment traveled between radial points was too large. For this reason, much of the data in this region are omitted from the results presented. The main difficulty in using the near field data is that the radial centerline of the flow field cannot be determined adequately. The centerline is determined by fitting the composition distribution with an exponential curve and using the center of the exponential curve as the centerline of the flow field. When there are insufficient data to define the curve, this procedure gives centerlines which are obviously in error.

A discussion of the probable accuracy of the experimental measurements is presented in Appendix A.

III. CONSISTENCY CHECK

The hydrogen mass flow was calculated at each axial station where data were obtained. The mass flux was numerically integrated to a specified control volume. The expression for the calculation is

$$\dot{W} = 2\pi \int_{o}^{R*} \rho u C R dR.$$

Numerous control volume sizes were tested. As long as the control volume was large enough to extend to a location where the hydrogen concentration was negligible, its size had little effect on the value obtained from the integration. The ratio of the values obtained from the integration [$\dot{W}$] to the hydrogen flow measured by metering orifice [$\dot{W}_j$] is shown in Figures 5 and 6. The results are reasonably good, considering that the hydrogen mass flow is only 0.4 to 1.7 per cent of the total mass flow in the mixing system.

A possible reason for a low calculated mass flow is that the probe was not on the vertical centerline when the data were recorded. There was no fixed reference point from which the vertical position measurements were made; therefore, only vertical position data recorded during the same test run may be compared. The data for tests I A and I D were recorded during the same test run;

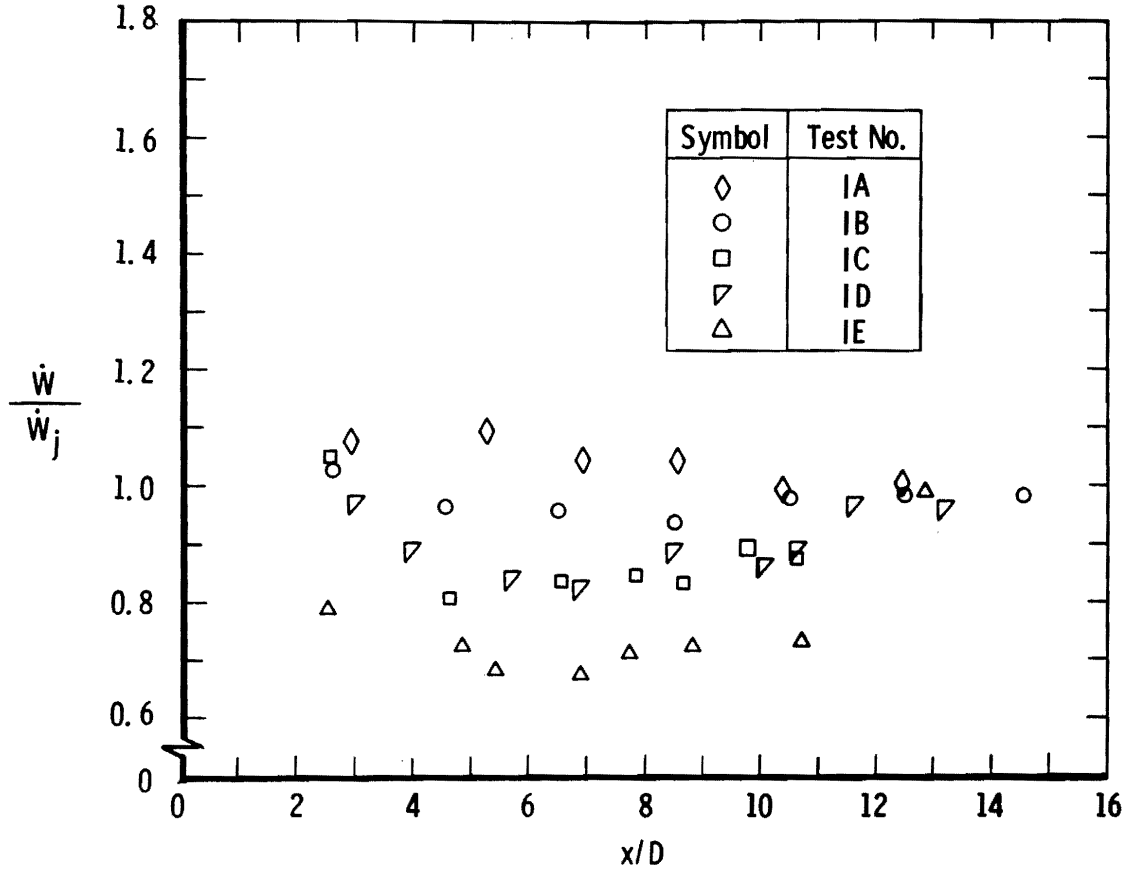

Figure 5. Consistency check for series I tests.

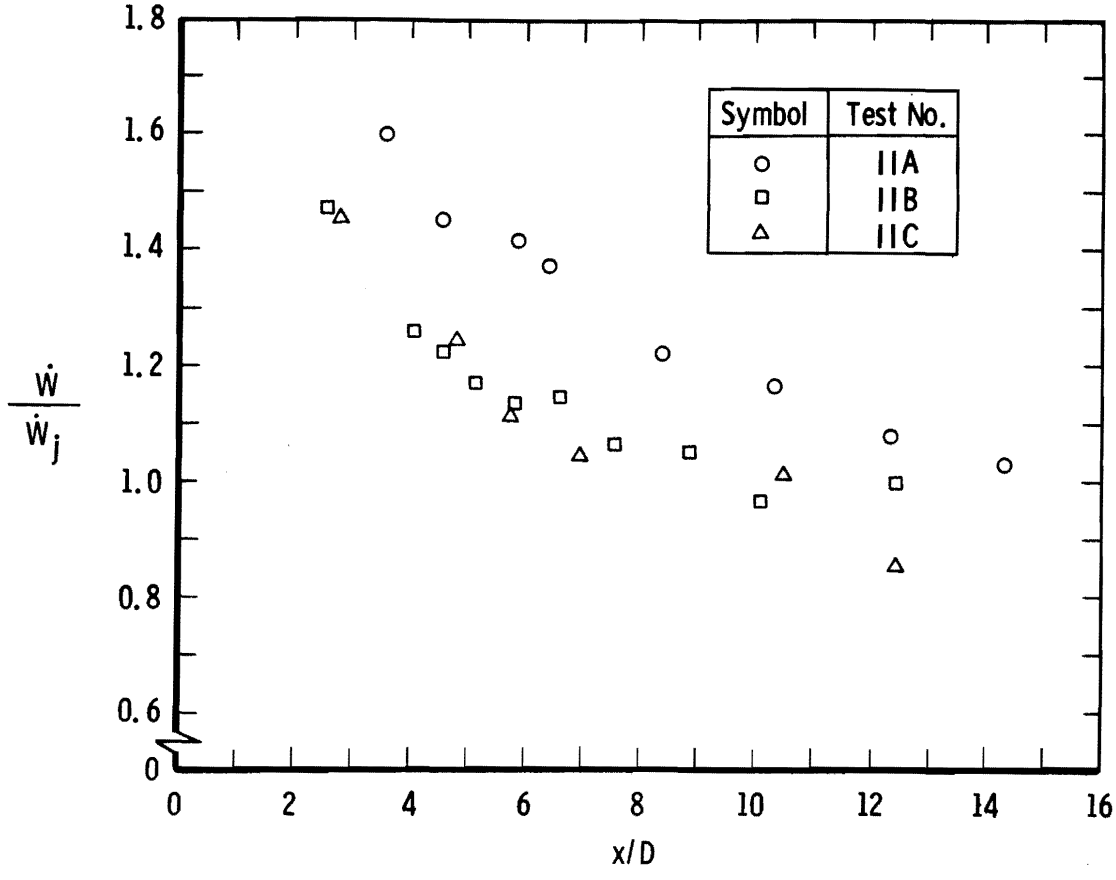

Figure 6. Consistency check for series II tests.

the vertical position variation between test I A and I D was 0.050 to 0.070 inch. Test I A gave good agreement on the consistency check, but test I D gave low values of mass flow calculated by the integration technique.

The following calculation was made to get an estimate of the effect of probe position error. The data from test I A were assumed to be on the true vertical centerline, and the integration was made for a traverse 0.060 inch below the centerline. The calculated change due to the assumed probe misalignment is from 2 to 5 per cent which is too small to account for the low values obtained during test I D.

The tests in Series II showed a trend toward high values of integrated mass flow near the nozzle exit plane; then the values decreased with increasing axial distance. The reason for this result is not known.

Even though the consistency check does give poor results for some tests on an absolute basis, the repeatability of the data is very good. All other data from tests which gave poor consistency checks agree well with the results for tests which gave good consistency checks. This fact is illustrated by the figures which present data from more than one test. The data appear to be better than the consistency check indicates.

IV. CENTERLINE DECAY

The centerline decay of composition and velocity for all hydrogen-air mixing tests is shown in Figures 7 and 8, respectively. These curves indicate that the centerline decay decreased with increasing velocity ratio for systems with approximately the same density ratio. The length of the potential core was determined by the method suggested by Zakkay (6). The centerline composition was plotted versus axial distance on logarithmic paper. A curve through the data was extrapolated until it intersected the line corresponding to 100 per cent jet gas concentration. It was assumed that the intersection defines the core length. A similar method was used to determine the velocity core lengths. The velocity core lengths were longer than the corresponding composition core lengths.

The density ratio of the inner jet gas to the outer stream gas was increased in Series II by heating the outer stream gas. The density ratio was increased even more in Series III by using air as the jet gas as well as the outer stream gas. Figure 9 presents a comparison of the centerline velocity decay for three different density ratios at approximately constant velocity ratio. The curves show that the centerline decay decreased with in-

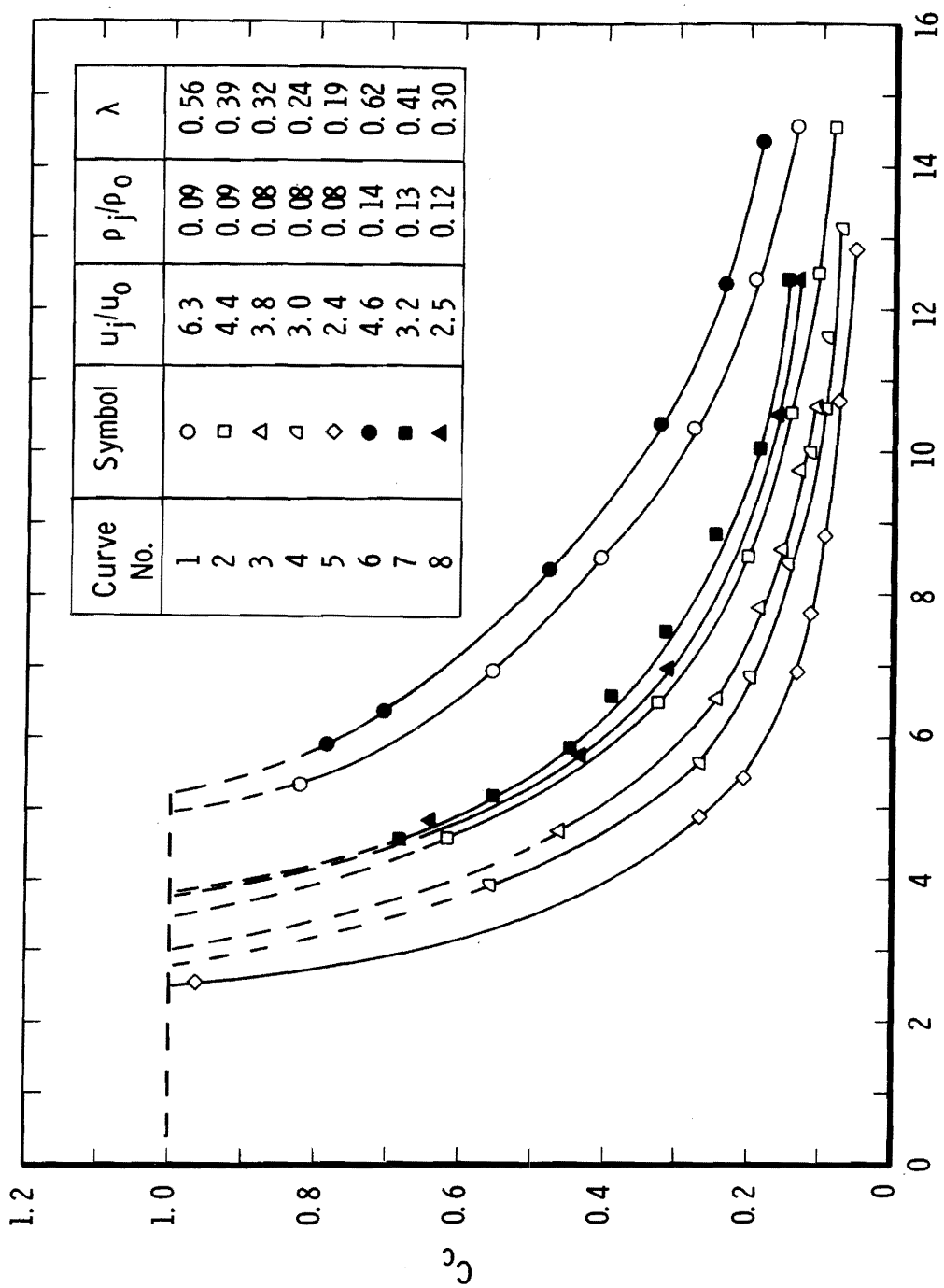

Figure 7. Centerline composition decay for the hydrogen–air tests.

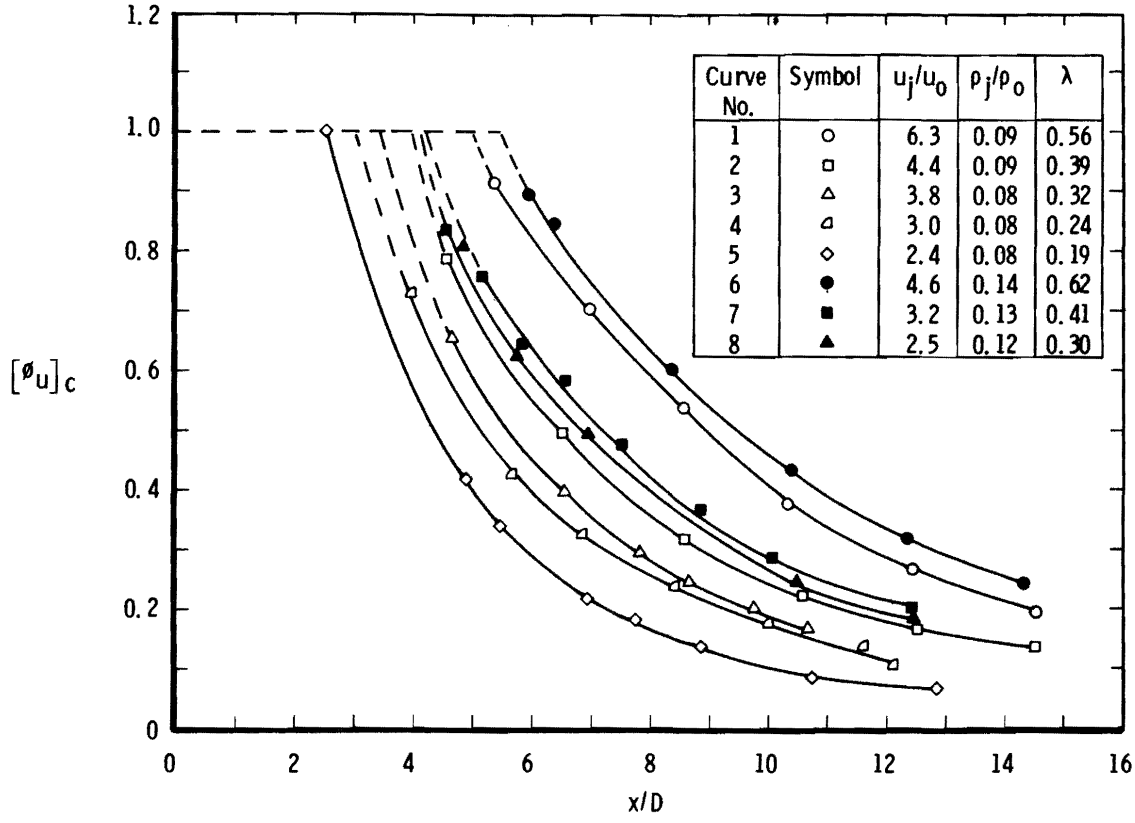

Figure 8. Centerline velocity decay for the hydrogen–air tests.

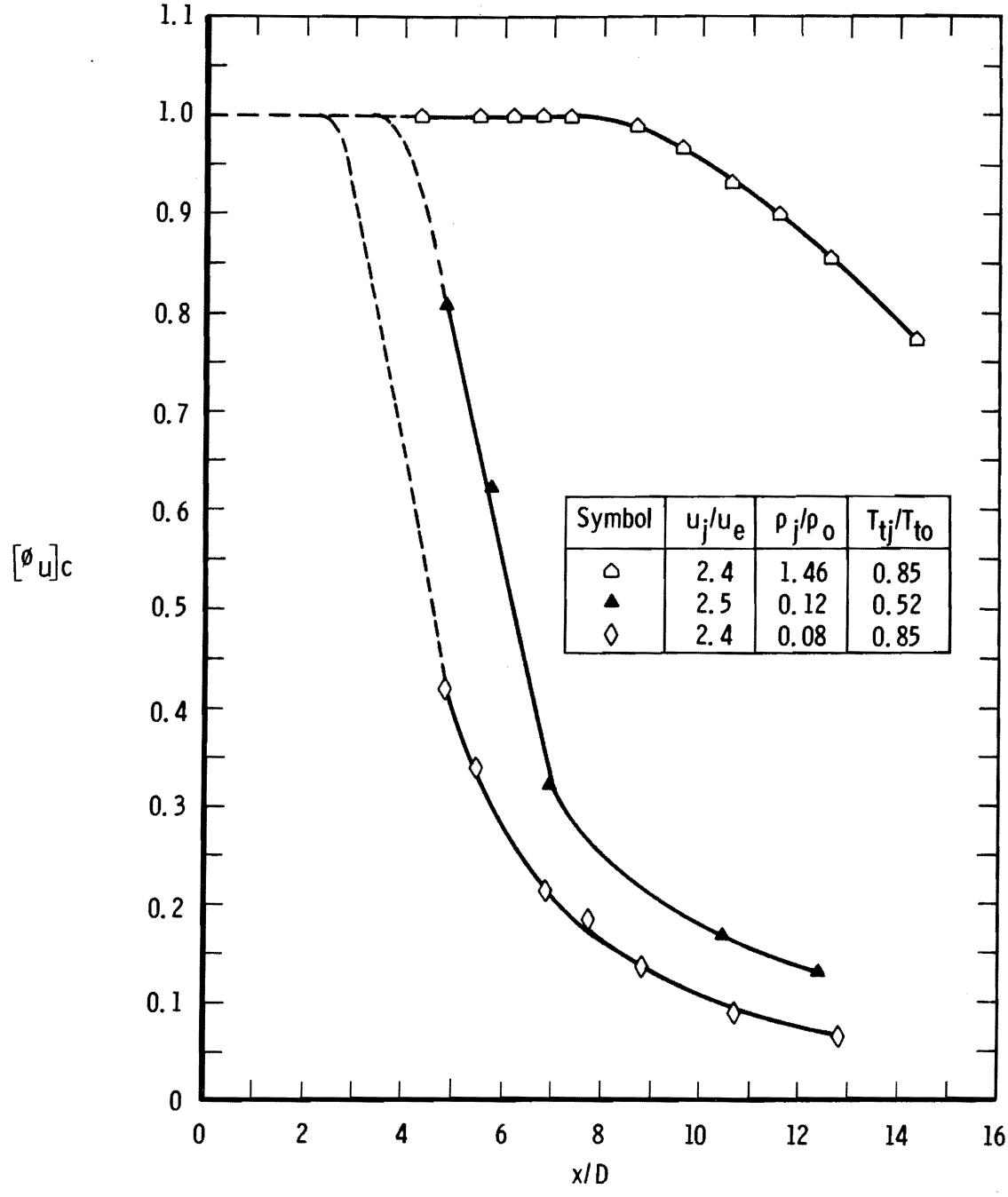

Figure 9. Centerline velocity decay for constant velocity ratio systems.

creasing density ratio for constant velocity ratio conditions. From the results presented, it is tempting to conclude that centerline decay decreases with increasing mass flux ratio. However, by considering curves 2, 3, and 8 in Figure 8, page 27, it is observed that this is not the case.

Zakkay and others (6) found the composition decay downstream of the potential core to follow the relationship $C_c \propto \frac{1}{\bar{x}^2}$. Figure 10 shows a comparison between Zakkay's results and the data from this investigation. By considering the expression $C_c \propto \frac{1}{\bar{x}^n}$, where Zakkay found n = 2, the results from this investigation gave n = 1.7. Zakkay also presented a generalized expression for potential core length variation with mass flux ratio. Figure 11 shows a comparison between Zakkay's generalized expression and data from this investigation. Zakkay's generalized expressions do not seem to apply in this higher velocity ratio regime; however, differences in the initial conditions, such as boundary layer thickness, may account for the discrepancies.

Figures 12 and 13 compare the centerline decay of composition, velocity, and total enthalpy for representative tests in Series I and II.

The composition and total enthalpy decay is approximately equal for all of the tests conducted. This

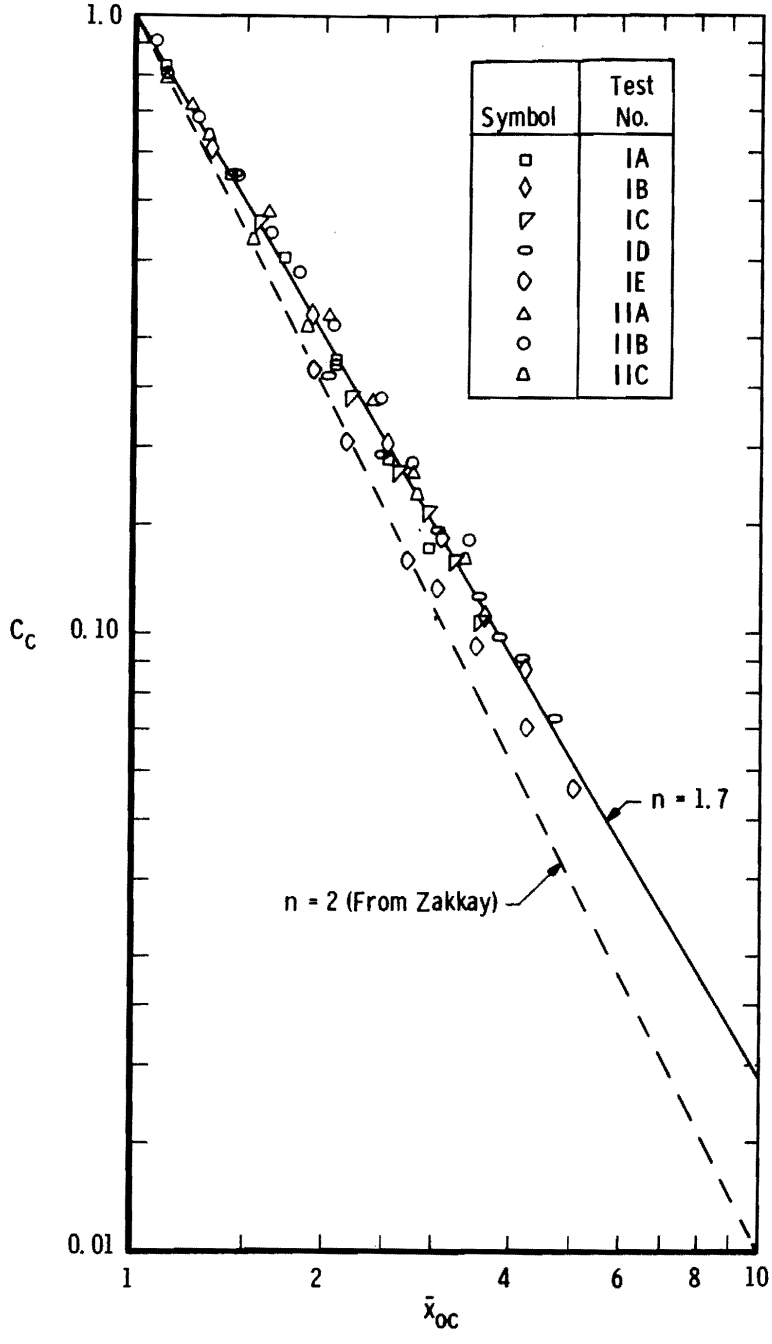

Figure 10. Centerline composition decay, comparison with Zakkay's result.

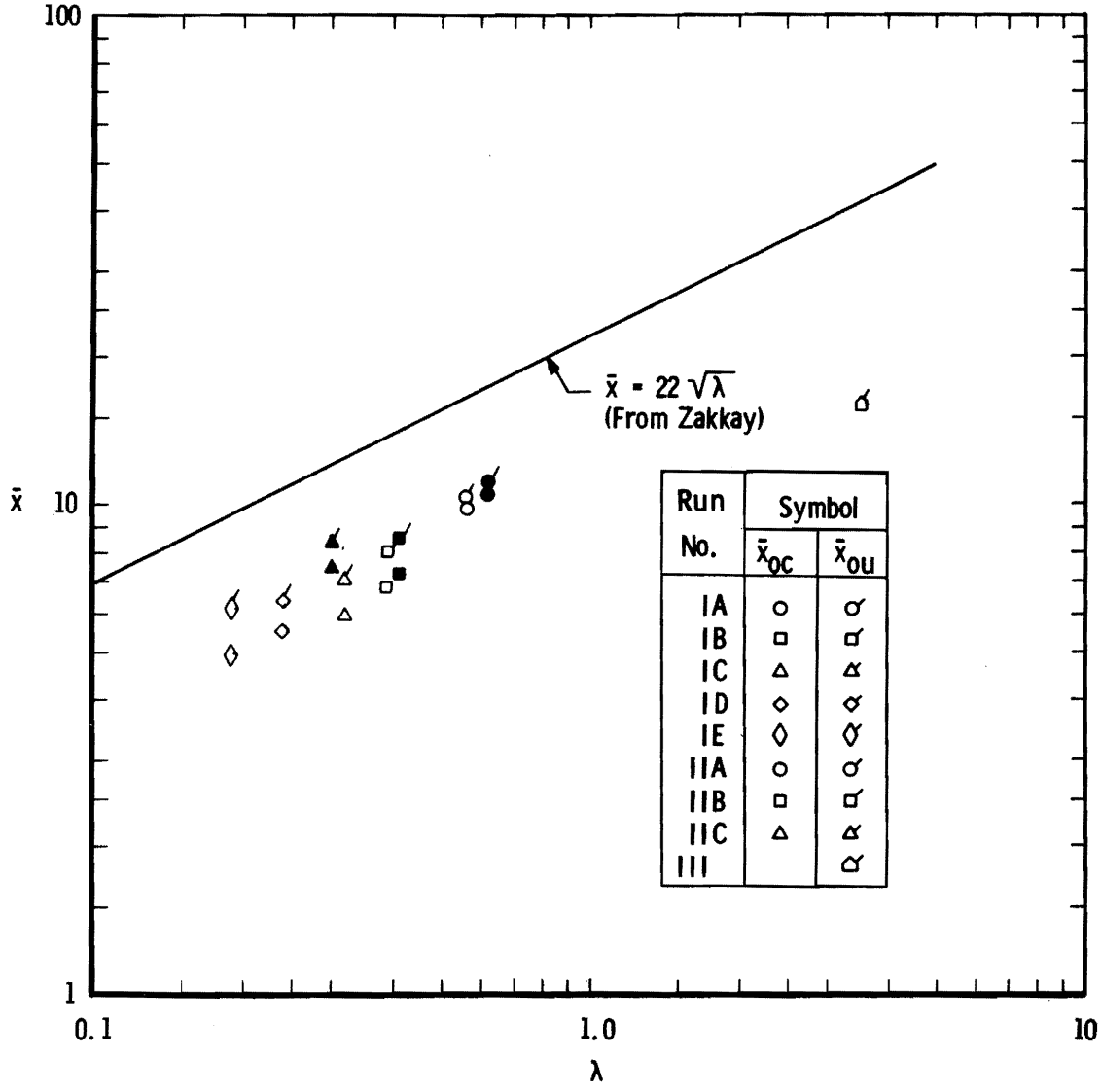

Figure 11. Potential core length versus mass flux ratio.

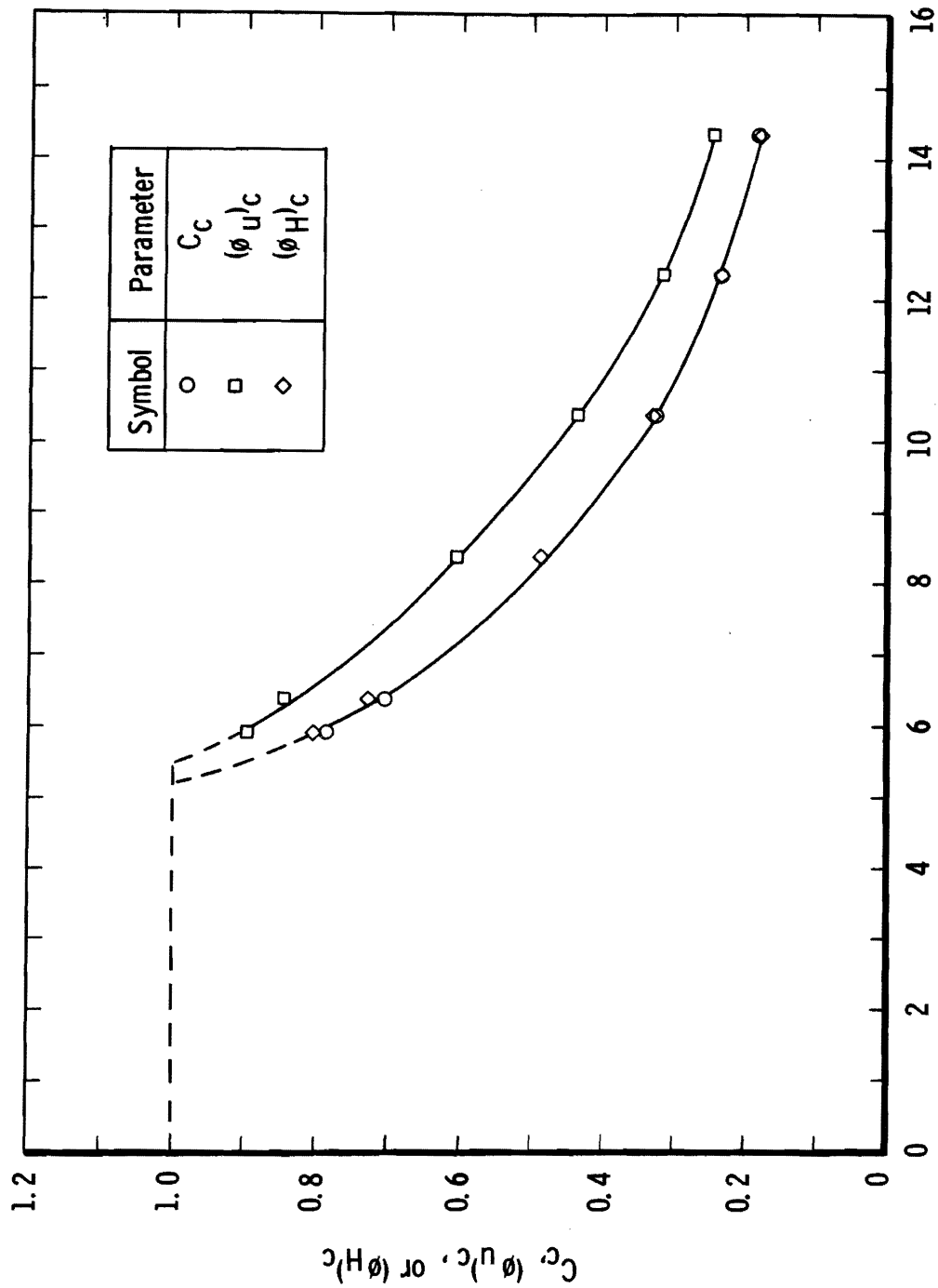

Figure 12. Centerline decay for test II A.

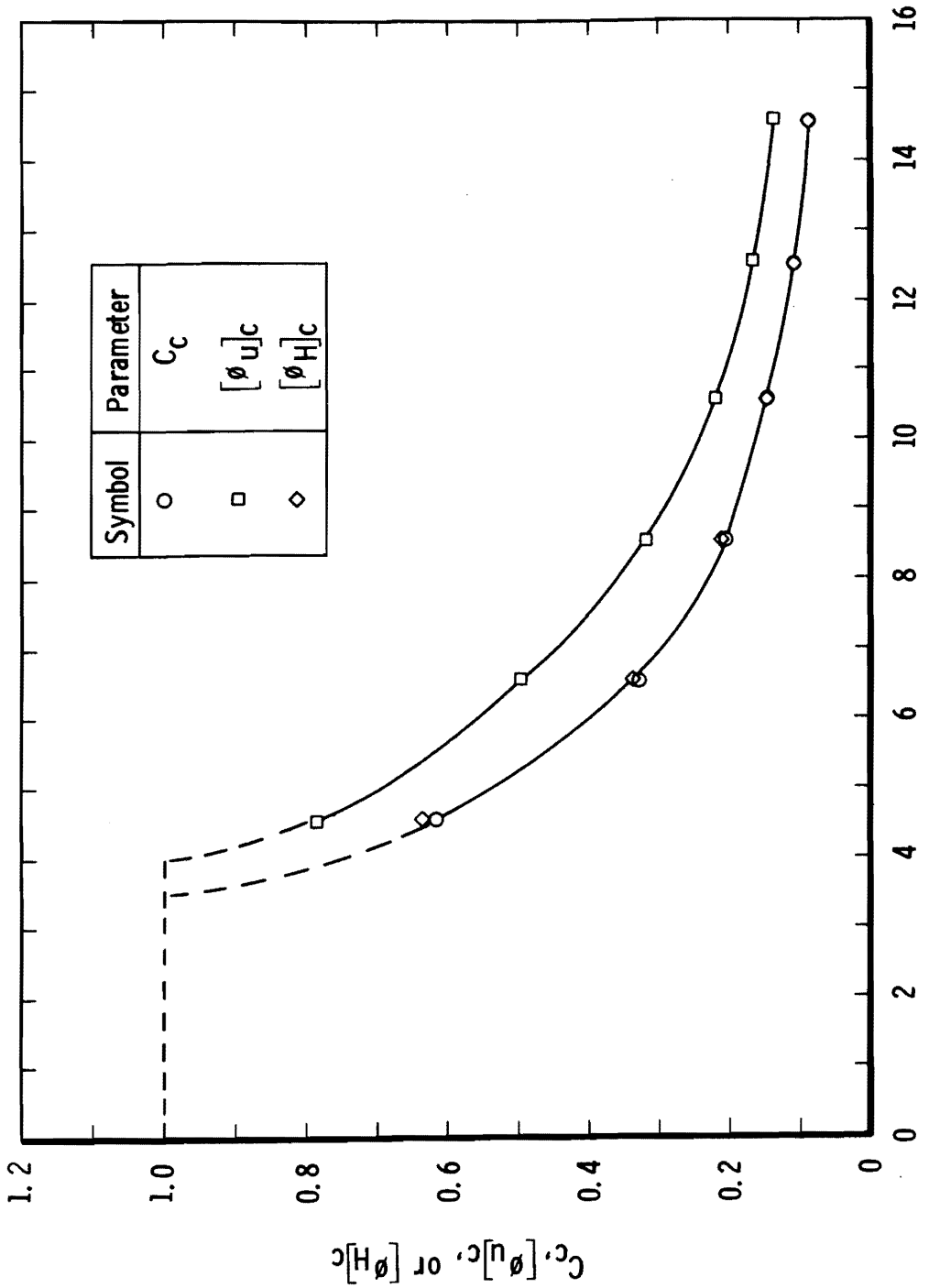

Figure 13. Centerline decay for test I B.

result may be expected in the Series I tests because the enthalpy calculation was a stronger function of composition than of temperature, and the temperature difference between the streams was only 100°R. But, in the Series II tests, the temperature difference was 500°R, and the effect of the turbulent transport properties should be important. Since composition and total enthalpy were equal for the Series II tests, the turbulent transport coefficients appear to be equal.

V. PROFILE SIMILARITY

The nondimensional composition for all of the hydrogen–air tests is plotted versus radial distance in Figure 14. The composition is nondimensionalized and normalized by dividing by the centerline composition. The nondimensionalized radius is obtained by dividing by the radius at which the composition is one–half of its centerline value. A band representative of the data in Figure 14 is presented in Figure 15. Curves obtained from three different mathematical functions are compared with the experimental data band. Each of the curves presented gives reasonably good agreement with the experimental data.

Nondimensional velocity is plotted versus radial distance in Figure 16. The parameters were nondimensionalized and normalized in a manner similar to those

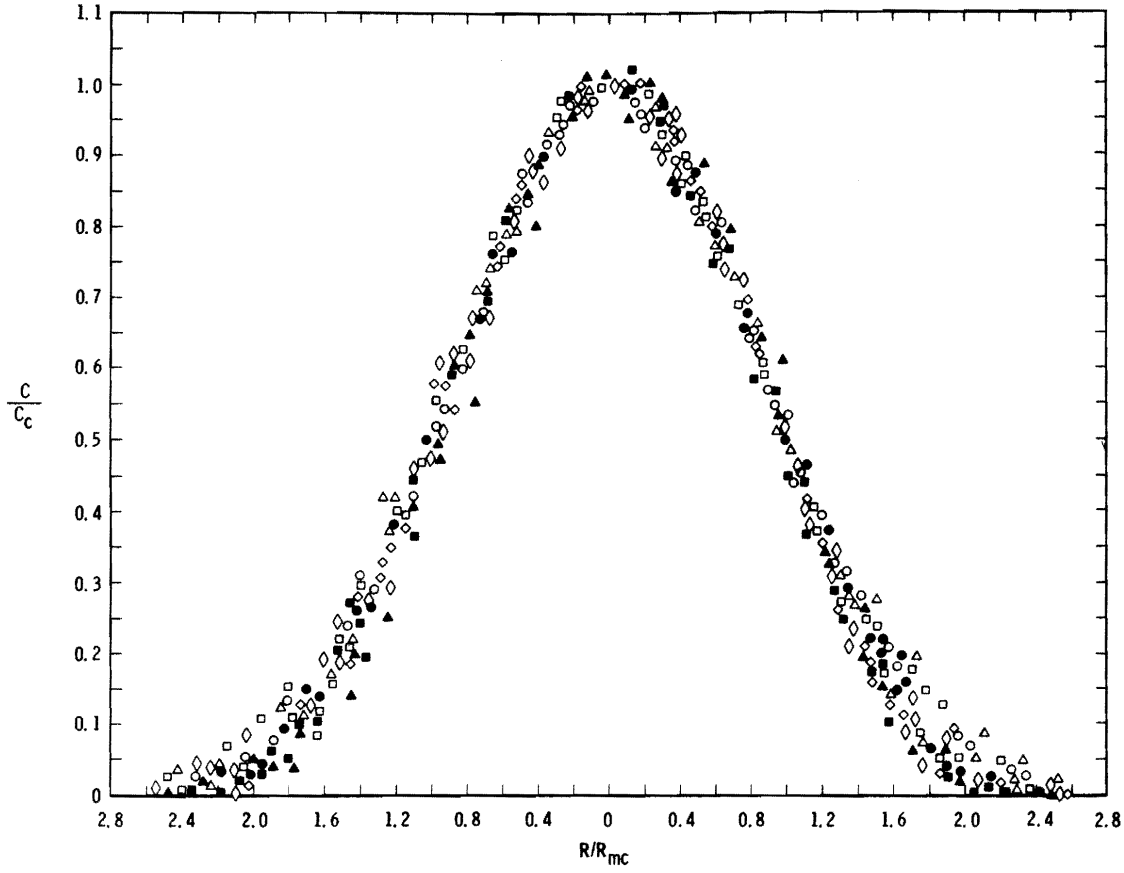

Figure 14. Radial composition profile.

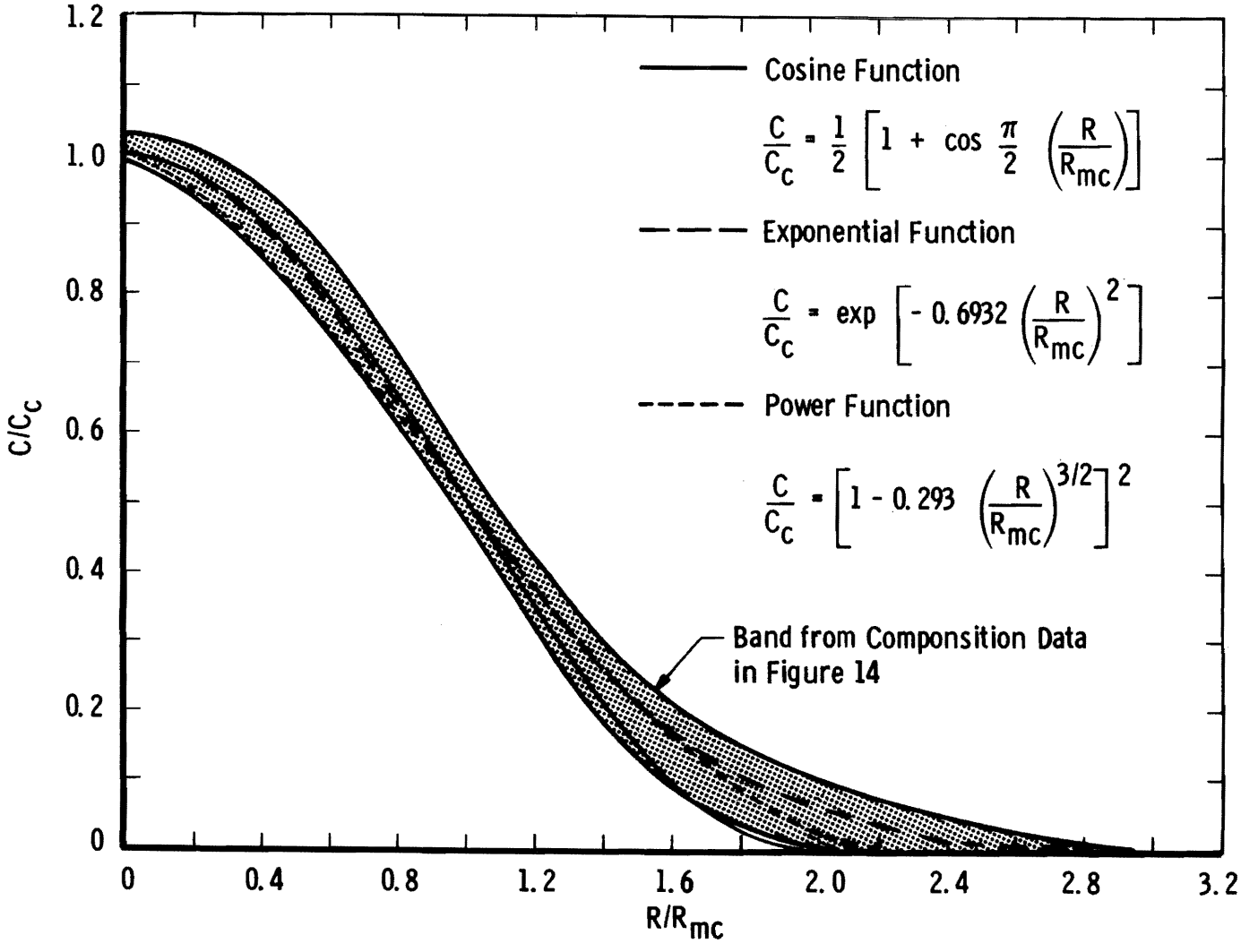

Figure 15. Radial composition profile, comparison with mathematical functions.

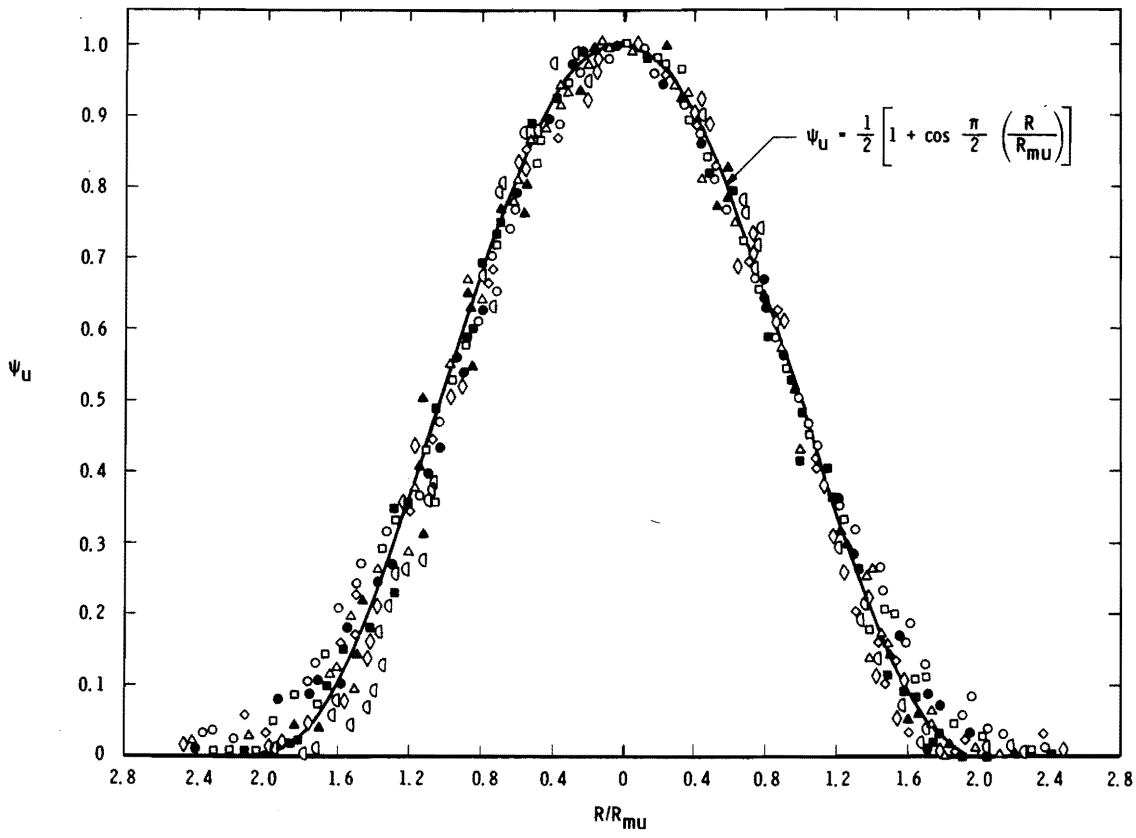

Figure 16. Radial velocity profile.

in Figure 14, page 35. The solid curve, which fits the data well, is the cosine function. The data in Figures 14 and 16 are representative of all test conditions and all axial locations. The curves indicate that profile similarity is an adequate assumption for engineering calculations in the velocity ratio range considered. The data outside R/R_{mc} and $R/R_{mu} = 2.5$ are not considered because the data in this region have a small hydrogen concentration, a small velocity difference, and consequently, a large uncertainty in the calculated values (see Appendix A). The mean radius values for composition and velocity are presented in Table II so that the actual radius values may be obtained from the curves in Figures 14 and 16.

Figure 17 presents a comparison between typical composition and velocity profiles from the same axial location for two different tests. The nondimensionalized composition and velocity are plotted versus radial distance. The composition profile is slightly wider than the velocity profile in each case.

In the first regime, it is generally accepted that

$$\frac{u - u_o}{u_j - u_o} = \frac{R - R_i}{b} .$$

TABLE II

NONDIMENSIONALIZING RADII

Test Number	x, ft	R_{mc}, ft	R_{mu}, ft
I A	0.22241	0.0173	0.0187
	.29077	.0196	.0197
	.3556	.0223	.0220
	.42922	.0262	.0253
	.51725	.0321	.0302
	.60815	.0430	.0344
I B	.18960	.0162	.0177
	.27100	.0220	.0213
	.35776	.0273	.0255
	.44036	.0331	.0306
	.52122	.0365	.0333
	.60479	.0400	.0367
I C	.19362	.0147	.0154
	.27354	.0217	.0201
	.32525	.0250	.0230
	.36195	.0266	.0240
	.40600	.0291	.0260
	.44526	.0309	.0273
I D	.12085	.0142	.0162
	.16597	.0178	.0143
	.23437	.0185	.0172
	.28599	.0207	.0186
	.35217	.0241	.0212
	.41687	.0273	.0231
	.44453	.0286	.0246
	.48473	.0295	.0258
	0.54896	0.0307	0.0287

TABLE II (continued)

Test Number	x, ft	R_{mc}, ft	R_{mu}, ft
I E	0.20282	0.0143	0.0132
	.22836	.0176	.0152
	.28768	.0196	.0162
	.32137	.0217	.0177
	.36891	.0229	.0172
	.44781	.0245	.0199
	.53378	.0276	.0200
II A	.19114	.0198	.0216
	.24602	.0202	.0208
	.26445	.0210	.0211
	.34731	.0237	.0226
	.43328	.0286	.0264
	.51582	.0320	.0297
	.59925	.0340	.0318
II B	.17055	.0169	.0196
	.18901	.0182	.0196
	.21611	.0192	.0192
	.24513	.0215	.0200
	.27351	.0231	.0208
	.31284	.0241	.0217
	.36946	.0273	.0243
	.41919	.0297	.0258
	.51784	.0332	.0282
II C	.20194	.0172	.0178
	.23974	.0195	.0180
	.29069	.0221	.0187
	.43775	.0270	.0232
	0.51780	0.0275	0.0228

TABLE II (continued)

Test Number	x, ft	R_{mc}, ft	R_{mu}, ft
III	0.28278		0.0251
	.30556		.0262
	.33236		.0266
	.36088		.0269
	.40028		.0269
	.44136		.0273
	.48228		.0280
	.52487		.0288
	0.59722		0.0315

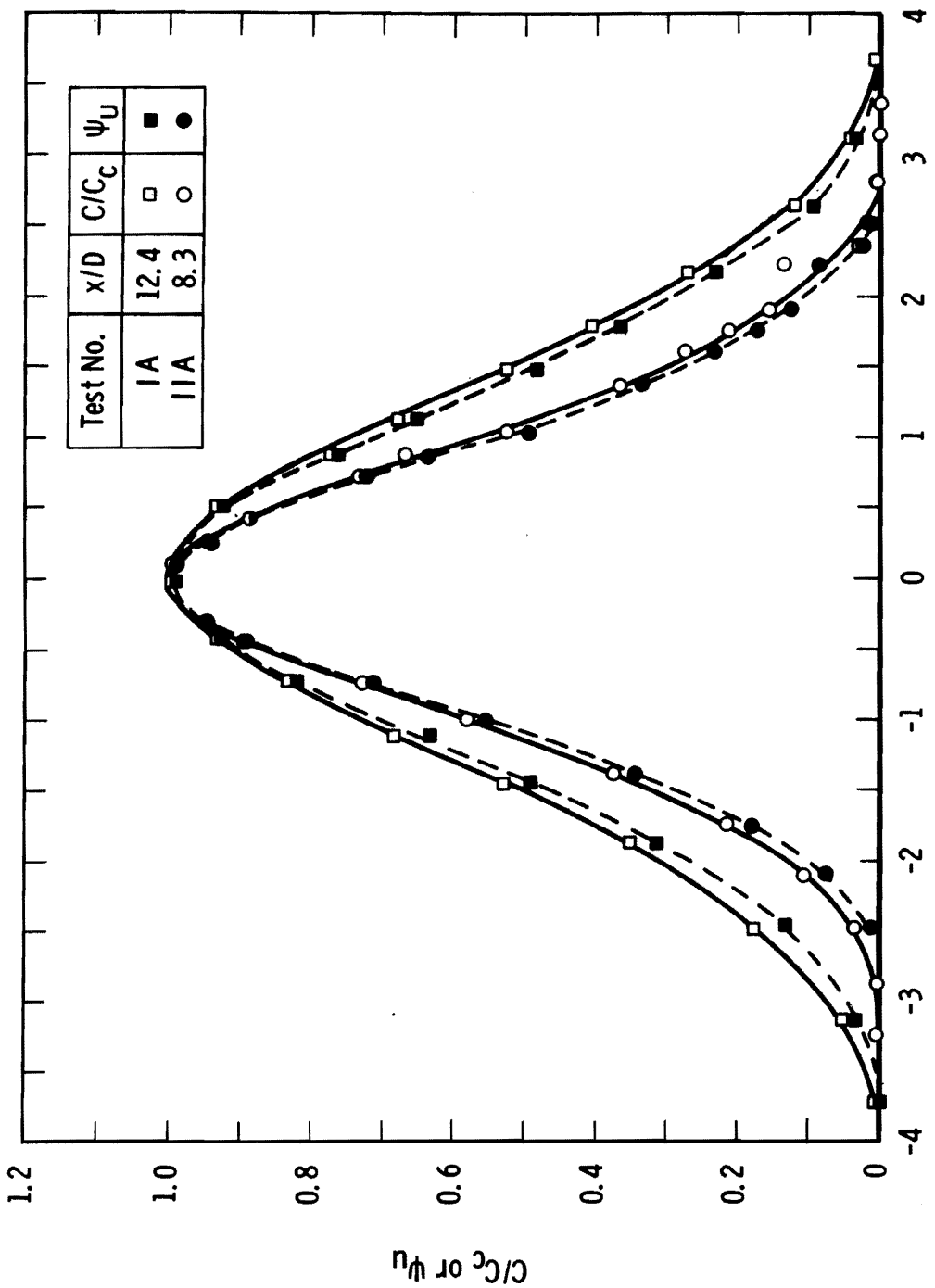

Figure 17. Radial composition and velocity profiles for tests I A and II A.

The term $[R_i]$ is the radius of the potential core where there is no velocity decay. Since it is very difficult to determine R_i or b accurately, the expression

$$\frac{R - R_{.9}}{R_{.1} - R_{.9}},$$

which is proportional to

$$\frac{R - R_i}{b},$$

is used in Figure 18 to illustrate velocity profile similarity. The solid curve is obtained from the expression,

$$\phi_u = \tfrac{1}{2}\left[1 + \cos \frac{\pi}{1.8}(R_B + 0.4)\right],$$

and agrees quite well with the data.

VI. MOMENTUM AND ENERGY TRANSPORT

In Figure 19, the nondimensionalized velocity is plotted versus the nondimensionalized enthalpy for all of the hydrogen–air tests. The velocity was nondimensionalized by using the jet velocity instead of the centerline velocity in this case. The dashed curve is the result for unity Prandtl number, and the deviation from it is indicative of the Prandtl number variation. These same parameters are plotted in Figure 20 for the air–air test, and a distinctly different trend is evident.

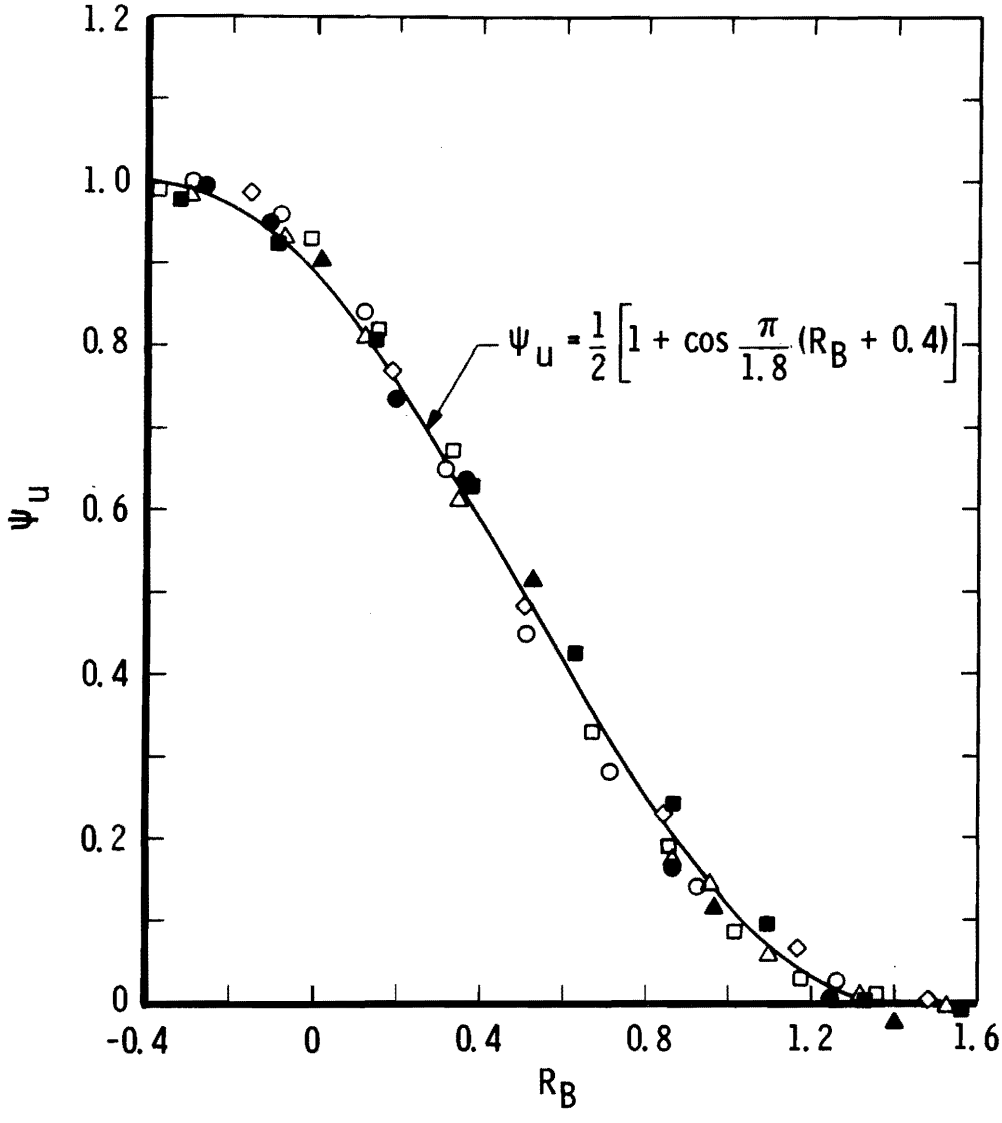

Figure 18. First regime radial velocity profile.

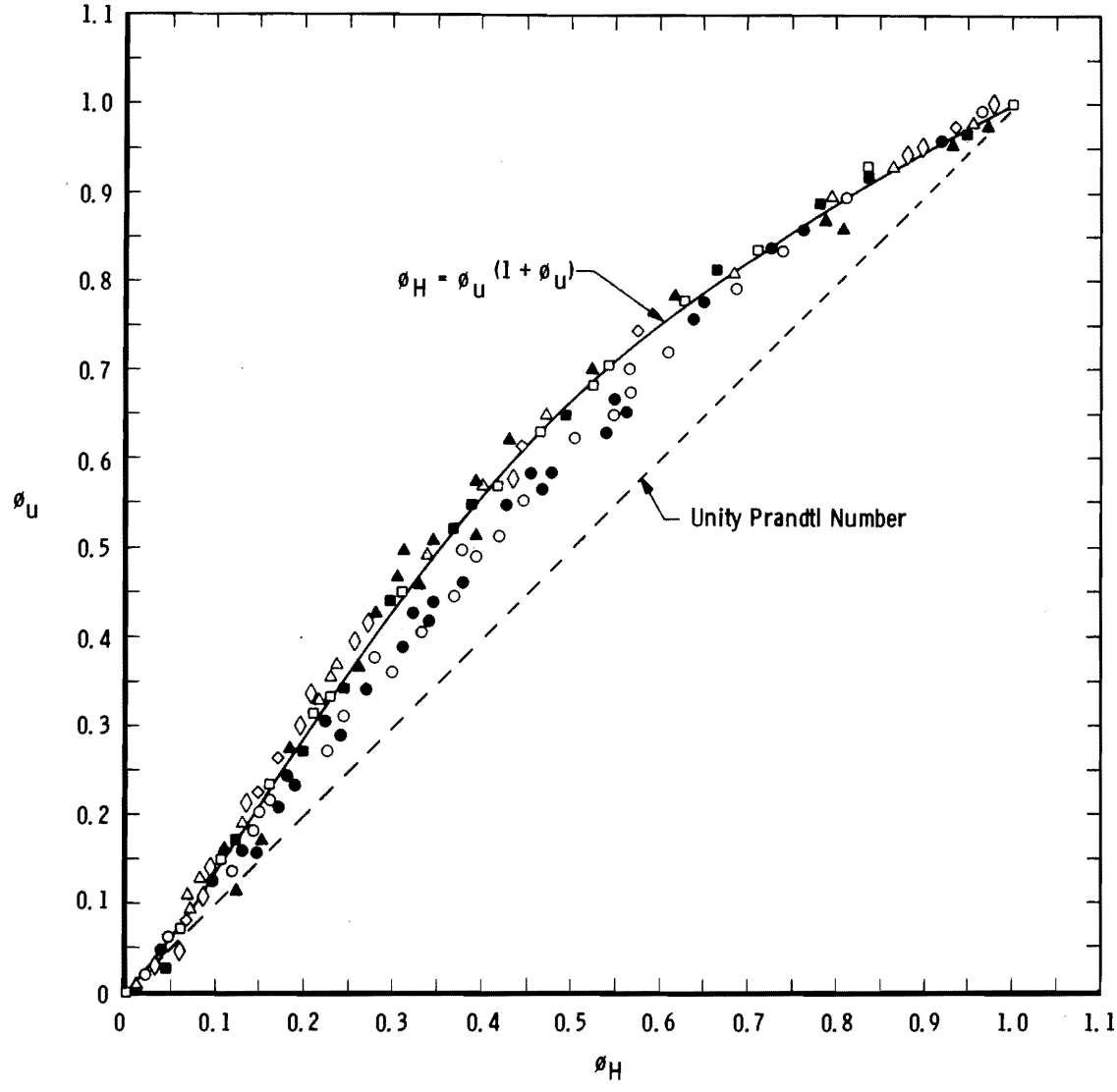

Figure 19. Velocity–enthalpy relationship for the hydrogen–air tests.

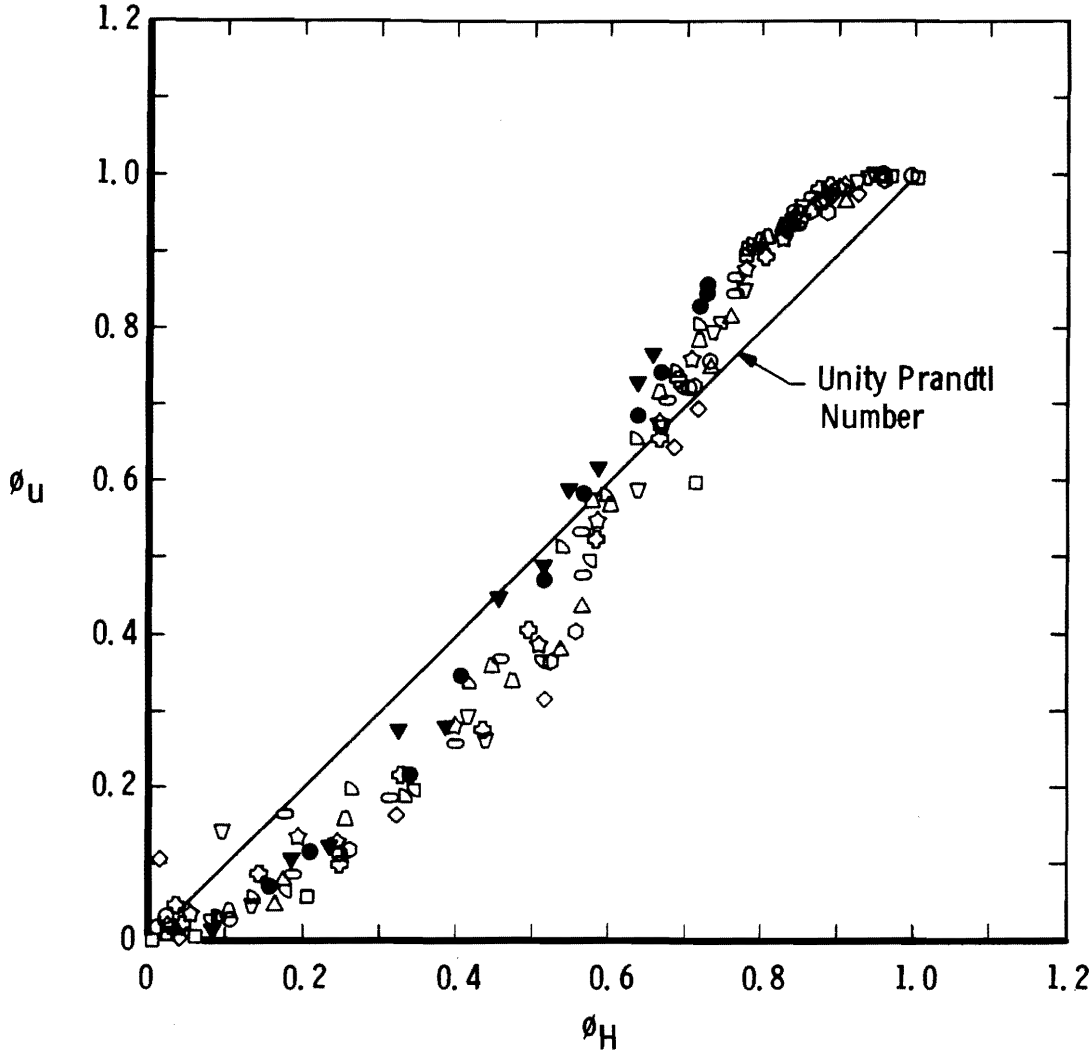

Figure 20. Velocity–enthalpy relationship for the air–air tests.

There appears to be a definite relationship between the transport of energy and the transport of momentum. However, it is not obvious how to estimate the Prandtl number from this relationship. A term of the form $[\phi_H = \phi_u^{Pr}]$ was suggested by Reichardt as presented by Schlichting (1) as a relationship between the transport of energy and the transport of momentum. The solid curve in Figure 19, page 45, was obtained from the expression $[\phi_H = \phi_u^{(1 + \phi_u)}]$, and it agrees reasonably well with the data. The part of this expression which corresponds to the Prandtl number in Reichardt's expression varies from 1 to 2.

VII. COMPOSITION AND ENERGY TRANSPORT

Composition is plotted versus nondimensionalized total enthalpy in Figure 21. The solid curve indicates the result for unity Lewis number. The experimental points deviate only slightly from the curve, which indicates that unity Lewis number is a good assumption for engineering calculations.

In all hydrogen-air tests, the turbulent transport of composition and total enthalpy is more rapid than the transport of momentum. This result is in agreement with other investigations reported (3, 4).

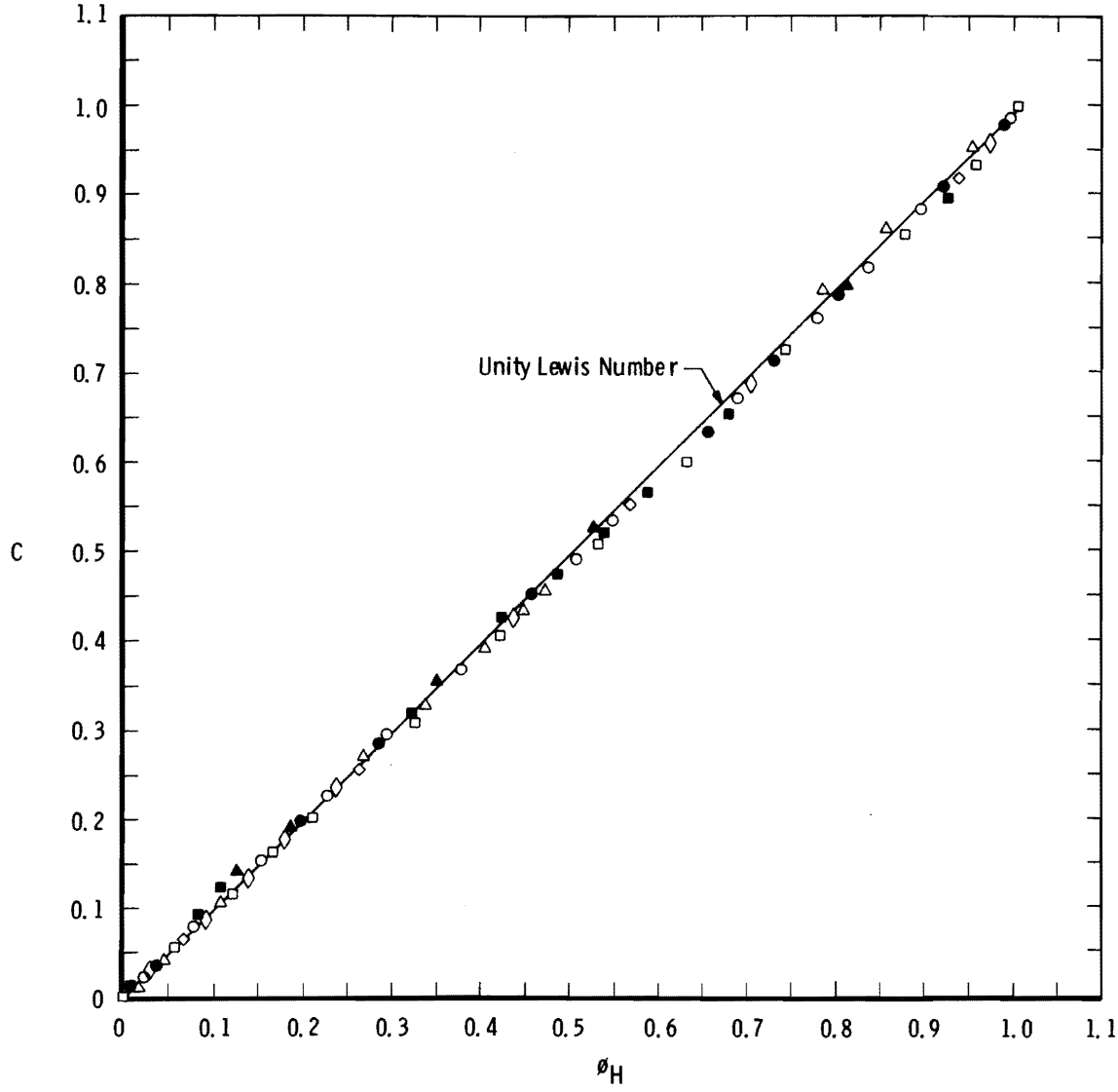

Figure 21. Composition–enthalpy relationship for the hydrogen–air tests.

VIII. STATIC PRESSURE

Typical static pressure distributions are presented in Figures 22 and 23. The pressure gradients are very large in the near field region; however, in a short distance, the gradients are smoothed to less than one per cent variation. The straight section at the nozzle exit is short, and the flow is not completely straightened when it enters the test section. If the flow is not normal to the axis of the static pressure probe, the probe will sense a total pressure component and give higher readings than expected. This is the most probable reason for the large static pressure gradients in the near field.

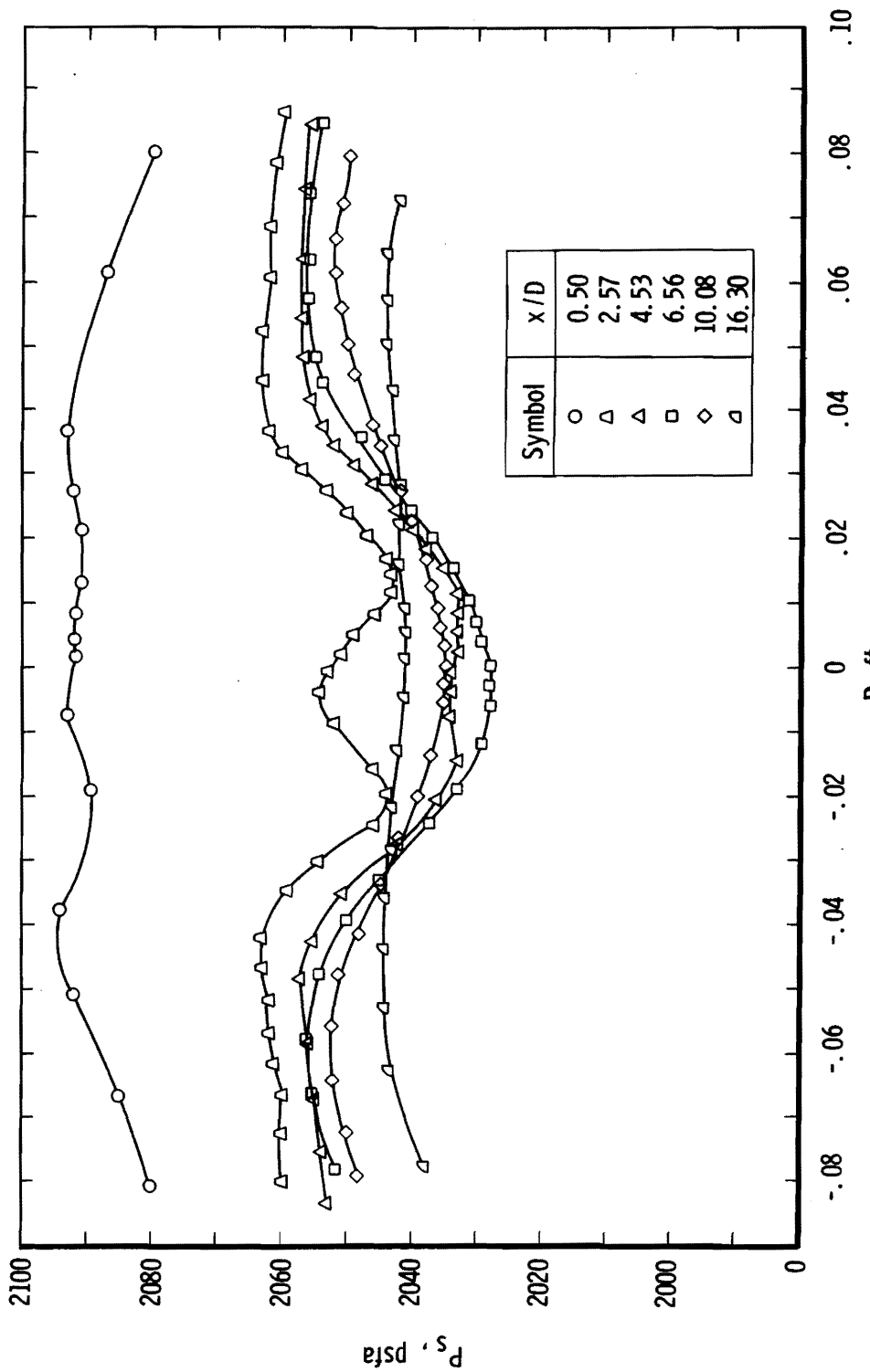

Figure 22. Static pressure profiles for test II B.

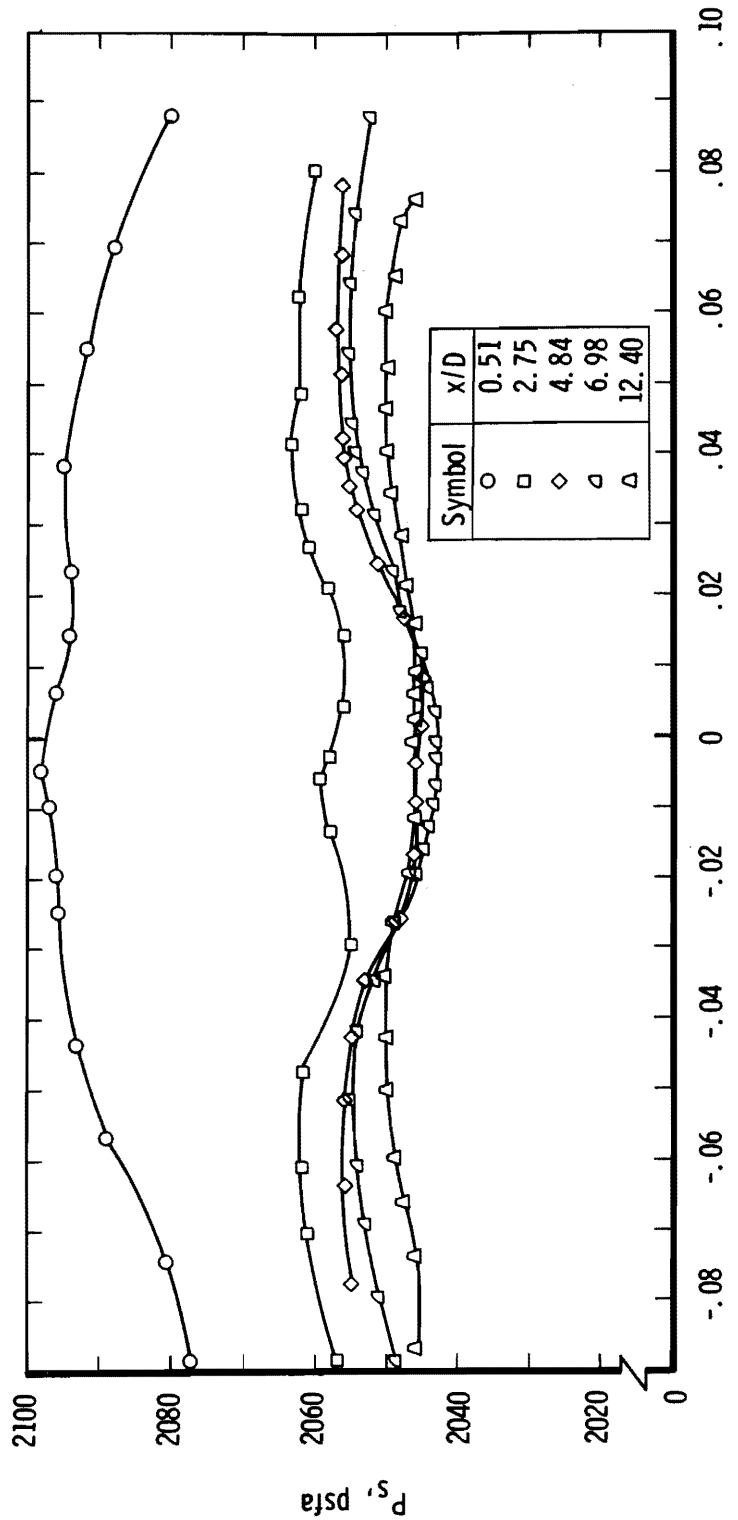

Figure 23. Static pressure profiles for test II C.

CHAPTER IV

CONCLUSIONS

The primary differences between this investigation and other investigations of turbulent mixing are that [1] the initial boundary layer effect was reduced by designing the nozzles to minimize the boundary layer buildup at the entrance to the test section, and [2] the velocity ratio range was higher than that previously reported.

The following conclusions may be drawn for subsonic, axisymmetric mixing, from this experimental investigation:

1. For hydrogen–air mixing systems, the centerline decay of composition and velocity decreased with increasing velocity ratio. Also, the centerline decay of composition and velocity decreased with increasing density ratio for constant velocity ratio systems. However, the centerline decay did not decrease monotonically with increasing mass flux ratio as it might appear from the preceding conclusions.
2. Similarity of composition, velocity, and total enthalpy profiles is a valid assumption for engineering calculations in the velocity ratio

range from 2.3 to 6.3 for hydrogen–air mixing systems. The commonly used expressions for the profile shapes, such as the cosine function, the three–halves power law, and the error curve, are representative of the shapes.

3. There appears to be a definite relationship between the transport of momentum and energy for hydrogen–air and air–air mixing systems. The relationship is such that the Prandtl number is not a constant, but the range of variation has not been determined.
4. Unity Lewis number is a valid assumption in the velocity ratio range considered, at least for streams which have moderate temperature differences.

CHAPTER V

RECOMMENDATIONS AND PLANS FOR FURTHER STUDY

A generalized theory for turbulent mixing is needed to solve many problems in fluid flow fields. A semi-empirical theory is probably the best approach that can be taken in the near future. The development of a semi-empirical theory will require a large amount of varied experimental data on different gas combinations and velocity ratios. The experimental tests, and especially the initial conditions, must be well documented to be of maximum value.

Additional work utilizing the existing data and test equipment is planned. The data will be further reduced to obtain shear stress distributions and turbulent transport coefficients. These results will be compared with other experimental and analytical results in an effort to obtain a model of eddy viscosity which is generally applicable. The existing test apparatus will be utilized to obtain data on [1] an air-air plus trace gas system, and [2] a chemically reactive hydrogen-air mixing system.

The test equipment will be modified to produce systems with large initial boundary layers. This equip-

ment will be utilized to study the effect of initial boundary layer thickness. Additional test equipment has been developed to study supersonic mixing systems.

BIBLIOGRAPHY

BIBLIOGRAPHY

1. Schlichting, H. Boundary Layer Theory. New York: McGraw-Hill Book Company, Inc., 1960.

2. Pai, S. I. Fluid Dynamics of Jets. New York: D. Van Nostrand Company, Inc., 1954.

3. Forstall, W., Jr. and A. H. Shapiro. "Momentum and Mass Transfer in Coaxial Gas Jets," Journal of Applied Mechanics, 17:399-408, December, 1950.

4. Alpinieri, L. J. "An Experimental Investigation of the Turbulent Mixing of Non-Homogeneous Coaxial Jets," Polytechnic Institute of Brooklyn PIBAL Report 789, Brooklyn, August, 1963.

5. Ferri, A., P. A. Libby, and V. Zakkay. "Theoretical and Experimental Investigation of Supersonic Combustion," High Temperatures in Aeronautics. New York: Pergamon Press, 1962, pp. 55-118.

6. Zakkay, V., E. Krause, and S. D. L. Woo. "Turbulent Transport Properties for Axisymmetric Heterogeneous Mixing," AIAA Journal, 2:1939-1947, November, 1964.

7. Peters, C. E., T. Peters, and R. B. Billings. "Mixing and Burning of Bounded Coaxial Streams," Arnold Engineering Development Center AEDC-TR-65-4, Arnold Air Force Station, Tennessee, March, 1965.

8. Mikhail, S. "Mixing of Coaxial Streams Inside a Closed Conduit," Journal of Mechanical Engineering Science, 2:59-68, 1960.

9. Keenan, J. H. and J. Kaye. Gas Tables. New York: John Wiley & Sons, Inc., 1954.

APPENDIXES

APPENDIX A

RELATIVE ERROR ANALYSIS

The measured parameters are listed in Table III with an estimate of the measuring accuracy.

In the following error equation, γ is assumed to be a constant. This assumption is justified by considering that the maximum deviation of γ from 1.4 is 1.7 per cent. This deviation was obtained when the outer air stream was heated to 1050°R.

The relative error equation for enthalpy is

$$\frac{dH}{H} = \left[\frac{C}{C + (1-C)\frac{H_a}{H_h}}\right]\frac{dH_h}{H_h} + \left[\frac{(H_h - H_a)}{H_h + (1-C)\frac{H_a}{C}}\right]\frac{dC}{C}$$

$$+ \left[\frac{(1-C)}{\frac{CH_h}{H_a} + (1-C)}\right]\frac{dH_a}{H_a} .$$

The relative error equation for density is

$$\frac{d\rho}{\rho} = \frac{-dT_t}{T_t} + \frac{\gamma - 1}{\gamma}\frac{dP_t}{P_t} + \frac{1}{\gamma}\frac{dP_s}{P_s} - \frac{26.95\ C}{26.95\ C + 2.016}\frac{dC}{C} .$$

TABLE III

MEASUREMENT ACCURACY

Parameter	Estimate of Measurement Accuracy Per Cent	Range
P_s	± 1	All Considered
P_t	± 1	All Considered
P_{tj}	± 1	All Considered
P_{to}	± 1	All Considered
T_t	± 0.5	All Considered
T_{tj}	± 0.5	All Considered
T_{to}	± 0.5	All Considered
R	± 2	All Considered
x	± 2	All Considered
C	± 2	0.05 to 1.0
C	± 10	0.02 to 0.05
C	± 50	0.01 to 0.02
C	Uncertain	0.0 to 0.01

The relative error equation for velocity is

$$\frac{du}{u} = \frac{1}{2}\frac{dT_t}{T_t} + \left[\frac{T_t}{T_s \gamma M^2} - \frac{\gamma-1}{2\gamma}\right]\frac{dP_t}{P_t} + \frac{13.98\ C}{26.95\ C + 2.016}\frac{dC}{C}$$

$$+ \left[\frac{\gamma-1}{2\gamma} - \frac{1}{\gamma M^2}\frac{T_t}{T_s}\right]\frac{dP_s}{P_s} \quad .$$

These equations are written for the mixing flow field conditions. They are applicable for the plenum conditions if the appropriate measured quantities are used.

The terms [R_{mc}, R_{mu}, and R_B] are selected from curve fits and do not depend on the measuring accuracy of a single point. It is estimated that they are accurate within ±3 per cent. Maximum errors in H, ρ, and u are given in Table IV for typical test conditions.

The relative error equation for ψ_u is

$$\frac{d\psi_u}{\psi_u} = \frac{u}{u - u_o}\frac{du}{u} - \frac{u_c}{u_c - u_o}\frac{du_c}{u_c}$$

$$+ \frac{u_o\,(u - u_c)}{(u - u_o)(u_c - u_o)}\frac{du_o}{u_o} \quad .$$

Table V presents the influence coefficients for the equation. The influence coefficients become large as u approaches u_o, and this trend is magnified as u_c approaches u_o. The parameter, ψ_u, is susceptible to large inac-

TABLE IV

ERRORS IN CALCULATED PARAMETERS

T_t	C	M	T_s/T_t	dT_t/T_t	dC/C	dP_s/P_s	dP_t/P_s	du/u	$d\rho/\rho$	H_h	H_a	dH_h/H_h	dH_a/H_a	dH/H
600	0.5	0.5	0.952	0.01	0.05	0.01	0.01	0.085	0.064	2021.6	143.5	0.02	0.02	0.063
↓	.5	.5	.952	↓	.02	↓	↓	.071	.038	↓	↓	.01	.01	.027
↓	.7	.7	.911	↓	.02	↓	↓	.044	.038	↓	↓	.01	.01	.028
↓	.05	.3	.982	↓	.1	↓	↓	.019	.060	↓	↓	.01	.01	.050
↓	.02	.3	.982	↓	.5	↓	↓	.218	.126	↓	↓	.02	.02	.124
↓	.02	.5	.952	0.005	.5	↓	↓	.114	.121	↓	↓	.01	.01	.114
↓	.05	.5	.952	↓	.1	↓	↓	.080	.055	↓	↓	.02	.02	.060
↓	.5	.5	.952	↓	.02	↓	↓	.069	.033	↓	↓	.02	.02	.037
↓	.9	.5	.952	↓	↓	↓	↓	.069	.034	↓	↓	.01	.01	.028
↓	.5	.7	.911	↓	↓	↓	↓	.041	.033	↓	↓	.04	.04	.057
↓	.3	.7	.911	↓	↓	↓	↓	.040	.031	↓	↓	.01	.01	.026
↓	.7	0.7	0.911	↓	↓	↓	↓	0.041	0.033	↓	↓	.01	.01	.028
1000	.02				.5					3405	241	0.01	0.01	.114
↓	.05				.1					↓	↓	↓	↓	.050
↓	.3				.02					↓	↓	↓	↓	.026
↓	.5				.02					↓	↓	↓	↓	.027
↓	.7				.02					↓	↓	↓	↓	.028
↓	.9				.02					↓	↓	↓	↓	.028
↓	.3				.05					↓	↓	↓	↓	.050
↓	0.7				0.05					↓	↓	↓	↓	0.055

TABLE V

INFLUENCE COEFFICIENTS FOR ψ_u

u_c, ft/sec	u_o, ft/sec	u, ft/sec	Influence Coefficients		
			$\frac{u}{u - u_o}$	$\frac{u_c}{u_c - u_o}$	$\frac{u_o(u - u_c)}{(u - u_o)(u_c - u_o)}$
3000	1000	2500	1.7	1.5	0.2
3000	1000	2000	2.0	1.5	0.5
3000	1000	1500	3.0	1.5	1.5
2000	1000	1800	2.3	2.0	0.3
2000	1000	1500	3.0	2.0	1.0
2000	1000	1200	6.0	2.0	4.0
1200	1000	1150	7.7	6.0	1.7
1200	1000	1100	11.0	6.0	5.0
1200	1000	1050	21.0	6.0	15.0

curacies when u approaches u_o near the outer edge of the mixing zone. For this reason, the uncertainty of the data outside $R/R_{mu} = \pm 2.5$ is very large, and the data are omitted from the curves presented. The same situation is true for the composition data. The low composition measurements, which have large measurement uncertainty, occur at the outer edge of the mixing zone. Consequently, the data outside $R/R_{mc} = \pm 2.5$ are omitted.

APPENDIX B

CALCULATION PROCEDURES

Gas mixture properties were calculated from the measured parameters by using the relationships listed below. Tables of specific heat and enthalpy for air and hydrogen over a temperature range from 500 to 1500°R were put into the computer program. The information was taken from gas tables (9).

Jet Mass Flow

$$\dot{W}_j = K_j \frac{P_{TH}}{\sqrt{T_{TH}}} ,$$

where K_j, a proportional constant, is furnished from the orifice calibration.

Total Enthalpy

$$H = CH_h + (1-C)\ H_a,$$

where H_h and H_a are obtained from the enthalpy table for the measured total temperature.

Molecular Weight

$$\omega = \frac{\omega_j\ \omega_o}{C(\omega_o - \omega_j) + \omega_j} .$$

Specific Heat

$$C_p = C(C_{pj}) + (1-C)\ C_{po},$$

where C_{pj} and C_{po} are selected from the table of specific heats for the total temperature.

Ratio of Specific Heats

$$\gamma = \frac{1}{1 - \frac{\bar{R}}{778\ C_p \omega}} .$$

Mach Number

$$M^2 = \frac{2}{\gamma-1} \left[\left(\frac{P_s}{P_t} \right)^{\frac{\gamma-1}{\gamma}} \right] - 1 .$$

Static Temperature

$$T_s = T_t\ (1 + \tfrac{\gamma-1}{2}\ M^2)^{-1} .$$

Density

$$\rho = \frac{P_s \omega}{\bar{R}\ T_s} .$$

Velocity

$$u = \sqrt{\gamma g (P_s/\rho) M^2} .$$